COMPUTATIONAL MODEL FOR PREDICTING BUCKLING IN RAIL STRUCTURES

A Thesis

by

VALENTINA MUSU

Submitted to the Office of Graduate and Professional Studies of
Texas A&M University
in partial fulfillment of the requirements for the degree of

MASTER OF SCIENCE

Chair of Committee,	David H. Allen
Committee Members,	Juan J. Horrillo
	Theofanis Strouboulis
Head of Department,	Sharath Girimaji

May 2021

Major Subject: Ocean Engineering

ABSTRACT

A model is developed herein for predicting the onset of thermally induced buckling in the horizontal and vertical planes for rail structures. As described below, the model may be considered to be an extension of previous efforts spanning most of the twentieth century, and particularly should be considered as an extension of the three degrees of freedom model presented in the CRR Report No. 2017-01 by D. H. Allen and G. Fry. Building on both previous analytic and computational solutions, a finite element model is developed for the purpose of predicting the thermal buckling temperature as a function of the track and support structure material properties, the track and support system geometries, the applied track loading, and the initial lateral displacement within the track. Particular emphasis is placed on nonlinearity and history dependence of the lateral track resistance to deformation. The resulting model is deployed herein to solve problems demonstrating usefulness of the model.

DEDICATION

“Fit via vi” – Ci si apre la strada con la forza

L’Eneide, Libro II, Virgilio

ACKNOWLEDGEMENTS

I would like to thank my committee chair, Dr. Allen, for his invaluable advice, support, and immeasurable patience as well as my committee members, Dr. Horrillo and Dr. Strouboulis, for their guidance and encouragement throughout the course of this research.

Thanks also go to my dear friend and colleague, LWC, without whom I would have never made it back to graduate school: you are my rock.

Finally, I would like to warmly thank all my friends and family that have stood by me and the choices I have made for my life: you know who you are, you are loved, and you are appreciated. Grazie, grazie, grazie.

CONTRIBUTORS AND FUNDING SOURCES

Contributors

This work was supervised by a thesis committee consisting of Dr. Allen and Dr. Horrillo from the Department of Ocean Engineering and Dr. Strouboulis from the Department of Aerospace Engineering.

This work should be considered an extension of the model presented in CRR Report No. 2017-01 by D. H. Allen and G. Fry published in 2017. Therefore, the work presented in Chapters I-V and Chapter VII was partially reproduced with the permission of the authors. The algorithm implemented into Python was partially translated from the FORTRAN original by Professor Cordes from the Department of Ocean Engineering.

All other work conducted for the thesis was completed by the student independently.

Funding Sources

Graduate study was supported by the means of a graduate research assistantship funded by Dr. Allen and the Transportation Technology Center Inc. (TTCI). The authors are grateful to the Association of American Railroads for the support provided for this research under PO #70490.

TABLE OF CONTENTS

Page

LIST OF FIGURES

Page

LIST OF TABLES

Page

CHAPTER I

INTRODUCTION*

Rails are known to undergo a variety of failure mechanisms that can cause significant property damage and loss of life (FRA 2020). It is therefore propitious to develop advanced models for the purpose of mitigating such mishaps. Toward this end, one such model is presented herein.

A common cause of rail misalignment is thermal buckling, as shown in Fig. 1. The Federal Railroad Administration (FRA 2020) reports that there have been 6,862 rail accidents within the United States in the last four years. Of these, approximately 0.7% are listed as being caused by rail buckling. However, an additional 10% of reported accidents may be related to thermal buckling such as broken rail bases (1.0%), buff/slack action excess (1.9%), kicking or dropping cars (2.2%), head shelling (2.3%), harmonic rock off (1.6%), and transverse/compound fissure (1.0%). These reported figures suggest that thermal buckling may be a causal factor in significant loss of life and damage costing perhaps as much as billions of dollars.

*Partially reproduced with permission from the authors, “Finite Element Formulation and Verification for Thermal Buckling of Rail Structures in the Horizontal Plane” by D Allen and G Fry [2017], CRR Report No. 2017-01

Figure 1 Photograph Showing Thermally Induced Buckling of a Railway (Reprinted with Permission from Allen and Fry, 2017)

Unfortunately, guidelines for mitigating the effects of thermal buckling have not to date been developed, and this is due to at least in part to the fact that thermal buckling is a rather complicated phenomenon caused by the following factors: temperature distribution within the rail, rail pinning, crosstie balance, lateral track walk, friction acting between the ties and the ballast, vertical lift-off and the structural configuration of the underlying railway base. Thus, there is a need to develop a technique for avoiding thermal buckling in rails.

The literature on this subject is long and deep. Historically, Galileo introduced the problem of a beam in bending in 1637 (Galileo 1637). More than a century later, the first cogent model for beam bending was reported by Euler and Bernoulli (Euler 1744). In the early twentieth century this approach was used to model the structural response of rails (Timoshenko 1915, 1927). Over the most recent half century a rigorous beam formulation

of the rail thermal buckling problem has emerged (Kerr 1974, 1978). This formulation presented has been utilized within the finite element method to predict lateral thermal buckling as a function of temperature, track residual deformation, nonlinear ballast interface resistance (Tvergaard and Needleman 1981). Nonlinear effects such as loss of contact between the rail and the wheel, rail lift-off from the tie and tie lift-off from the ballast have also been modelled (Dong, Sankar and Dukkipati 1994). Additionally, a continuous effort has been made to investigate the stability of continuously welded rail (CWR) (Kish, Samavedam and Jeong 1985, Kish, Kalay, Hazell, Schoengart and Samavedam 1993, Kish, Clark and Thompson 1995, Kish and Samavedam 1997 and 2005, Kish, Samavedam and Wormley 2001, and Klaren and Loach 1965) and the effects of thermal buckling in rails (Kish and Samavedam 1982, 1990, 1991, 1999 and 2013, Kish, Sussman and Trosino 2003 and Kristoff 2001). Furthermore, models excluding vehicle loads effects, also called static models, were developed for tangent and curved track with misalignments (Samavedam 1979, Kish and Samavedam 1991). Finally, further research was conducted to develop a dynamic model of track thermal buckling and stability (Samavedam, Kish and Jeong 1986 and 1987, Samavedam, Purple, Kish and Schoengart 1993, Samavedam 1995 and 1997, Samavedam, Kanaan, Pietrak, Kish and Sluz 1995, Samavedam et al. 1997 and Samavedam and Kish 2002).

More recently, a more detailed finite element formulation has been employed to include the effects of both fastener stiffness and vertical deformations on the prediction of lateral thermal buckling (Lim et al 2003). Furthermore, an analytical model has been developed for predicting the effects of tie and fastener resistance on lateral thermal

buckling (Grissom and Kerr 2006). Geometric nonlinear models have been developed for thermal buckling and nonlinear post-buckling of Euler-Bernoulli beams supported on elastic foundations and evaluated by shooting method (Li and Batra 2007, Yang and Bradford 2016). Lastly, complex three-dimensional models of continuously welded rail (CWR) have been developed using commercially available FE codes for buckling analysis of tracks subjected to thermal loading under a variety of different assumptions: linear friction (Pucillo 2016), interspersed railway tracks (Kaewunruen et al. 2018) multi-body dynamic interaction in consideration of nonlinear friction and uplift of the track (Miri et al. 2021).

Therefore, it is clear that there exists a need to develop a model that is capable of simulating the response of the rail due to thermal buckling when geometric nonlinearity, elastic foundation, track uplift and nonlinear friction occurring at the ballast-rail interface are incorporated simultaneously. The current research is focused on making use of the significant findings reported above to develop a model that is both convenient to deploy and capable of accurately predicting lateral thermal buckling in rails in the vertical and horizontal planes.

CHAPTER II

MODEL DEVELOPMENT*

Consider a generic rail mounted on a railway, as shown in Fig. 2. Note that the x coordinate axis is aligned in the direction of travel, and the y and z coordinate axes are aligned with the horizontal and vertical directions, respectively, thereby resulting in a right-handed coordinate system. Note that as a result of the right-handed coordinate system hereby described, a right-handed sign convention was also adopted throughout the development of the model, such that a counterclockwise rotation in in the x-y plane is considered positive, while a positive rotation in the x-z plane is by convention clockwise.

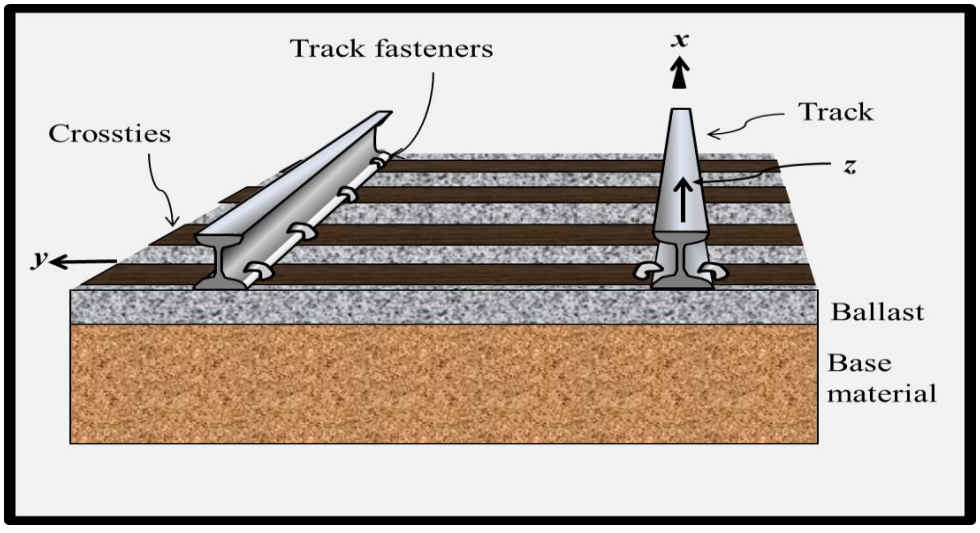

Figure 2 Generic Rail with Right-Handed Coordinate System as Shown (Reprinted with Permission from Allen and Fry, 2017)

*Partially reproduced with permission from the authors, "Finite Element Formulation and Verification for Thermal Buckling of Rail Structures in the Horizontal Plane" by D Allen and G Fry [2017], CRR Report No. 2017-01

When viewed in the horizontal plane, a typical rail with mechanical and thermal loading is shown in Fig. 3.

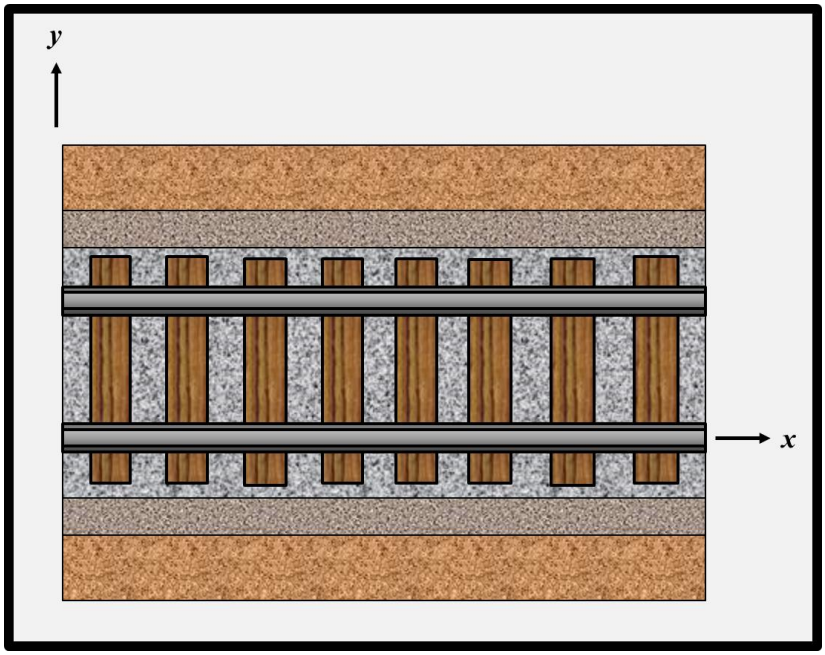

Figure 3 Horizontal View of Typical Rail Loaded Mechanically and Thermally (Reprinted with Permission from Allen and Fry, 2017)

In order to construct a model for thermal buckling of the track structure, it is assumed that the structure may be adequately modeled as a Euler-Bernoulli beam-column, implying that it is long and slender (Euler 1744, Allen and Haisler1985, Grissom and Kerr 2006). Furthermore, as Lim and coworkers (Lin et al. 2003) have shown that the out-of-plane deformation component might be significant, it will be assumed herein that this component of deformation must be included in the model to accurately predict lateral thermal buckling. Using these two assumptions, the track structure shown in Fig. 3 may be idealized as a single slender beam, as shown in Fig. 4. As shown in the figure, the

centroidal axis of the rail may deform in all three coordinate directions, and the components of this displacement are denoted by $u(x,t)$, $v(x,t)$ and $w(x,t)$, respectively. Similarly, the components of stress $\sigma_{xx}(x,y,z,t)$, $\sigma_{xy}(x,y,z,t)$ and $\sigma_{xz}(x,y,z,t)$ are shown on an arbitrary cross-section of the rail in Fig. 5.

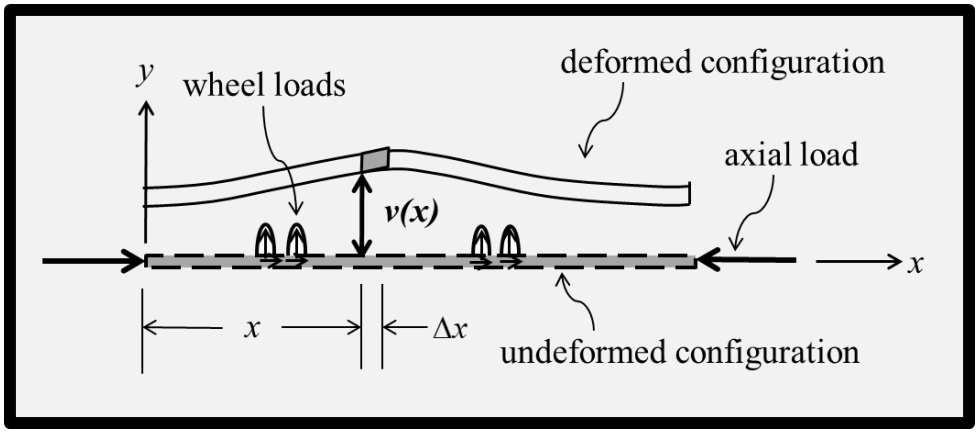

Figure 4 Top View of the Rail Showing Horizontal Transverse Displacement Component in the Deformed Configuration (Reprinted with Permission from Allen and Fry, 2017)

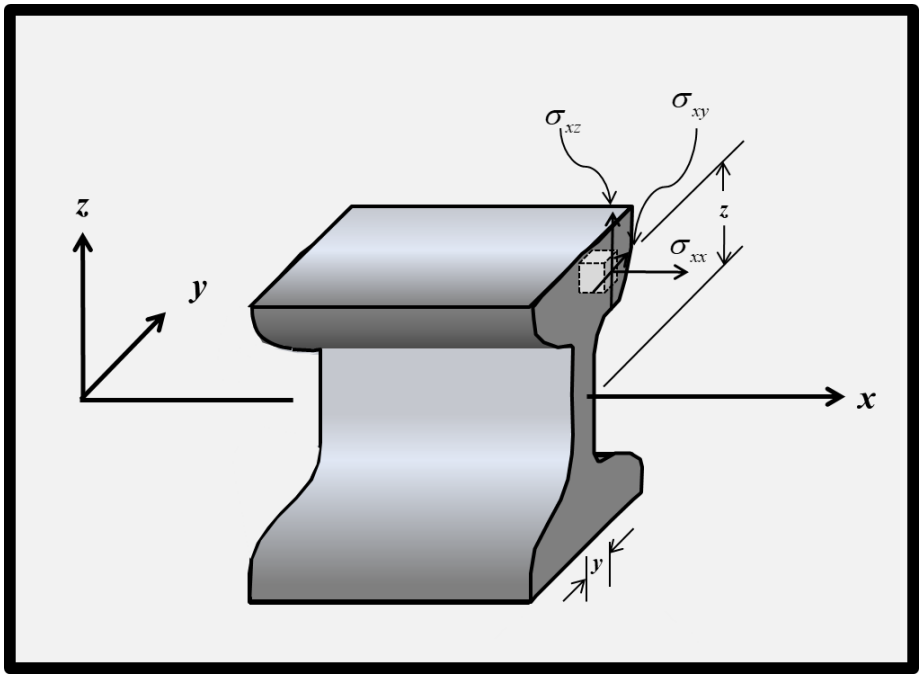

Figure 5 Components of Stress on an Arbitrary Cross-Section of the Rail (Reprinted with Permission from Allen and Fry, 2017)

A top view of a free body diagram of a section of the rail is constructed in Fig. 6, wherein the load per unit length applied to the centroidal axis of the rail is composed of components $p_x(x,t)$ and $p_y(x,t)$ in the *x* and *y* coordinate directions, respectively. In addition, the normal component of force per unit length applied to the bottom of the rail due to the normal displacement component $v(x,t)$ is denoted as $-k_y v(x,t)$, where $k_y(x,t)$ is the lateral coefficient of friction and the negative sign is employed so that the base stiffness is non-negative when the resultant is positive due to downward displacement of the rail. Similarly, the axial component of force per unit length applied to the bottom of the rail due to the axial component of displacement $u(x,t)$ is denoted as $-k_x u(x,t)$, where $k_x(x,t)$ is the axial coefficient of friction.

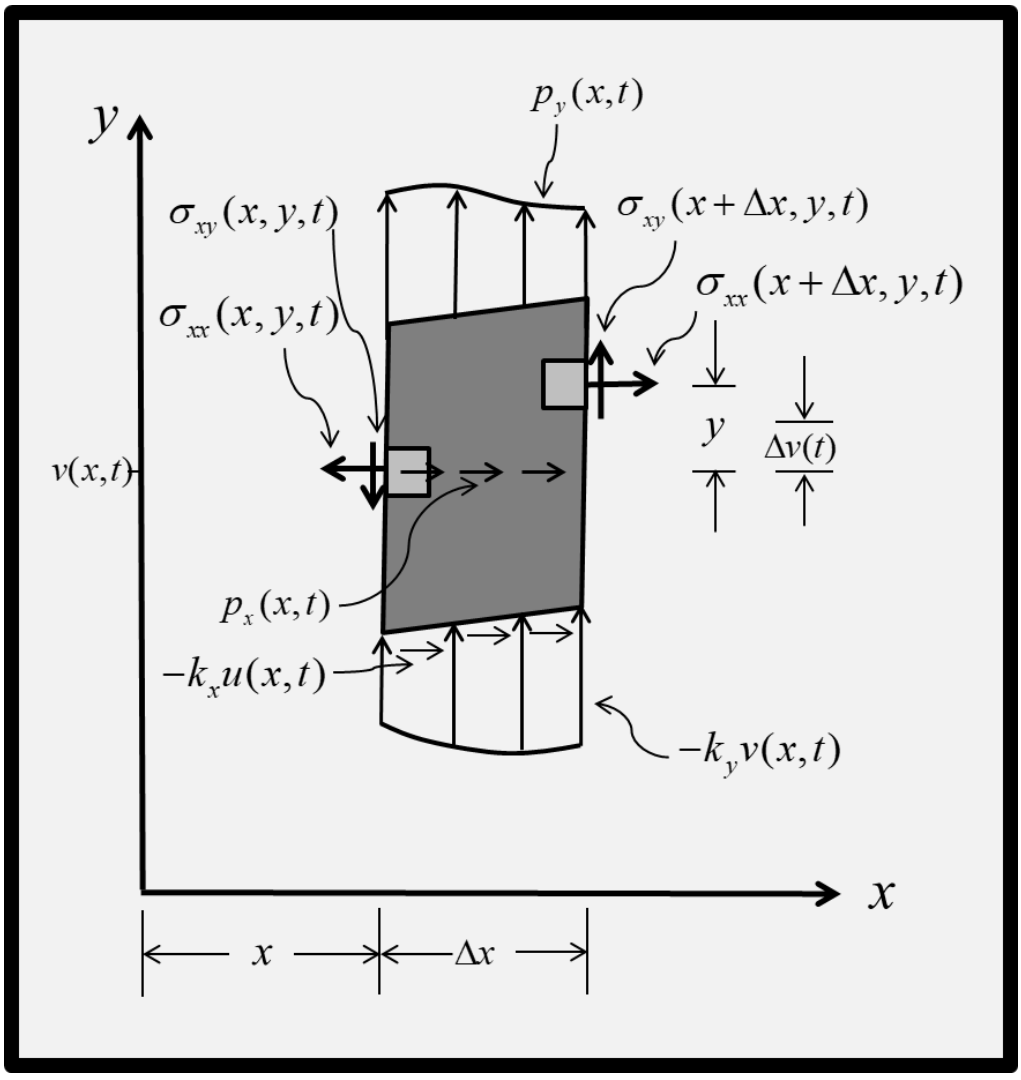

Figure 6 Top View of Free Body Diagram of Cut Rail (Reprinted with Permission from Allen and Fry, 2017)

Note also that the stress distribution on the two vertical cuts within the rail are denoted generically by the two infinitesimal stress boxes on these faces. Finally, note that the differential element is depicted in the deformed configuration, so that the axial force affects the transverse displacement of the rail. This necessarily causes the response of the rail to be geometrically nonlinear.

A side view of a free body diagram of a section of the rail is constructed in Fig. 7, wherein the load per unit length applied to the centroidal axis of the rail is composed of components $p_x(x,t)$ and $p_z(x,t)$ in the x and z coordinate directions, respectively. In addition, the out-of-plane component of force per unit length applied to the bottom of the rail due to the out-of-plane displacement component w(x,t) is denoted as $-k_z w(x,t)$, where $k_z(x,t)$ is the vertical coefficient of friction and the negative sign is employed so that the base stiffness is non-negative when the resultant is positive due to downward displacement of the rail.

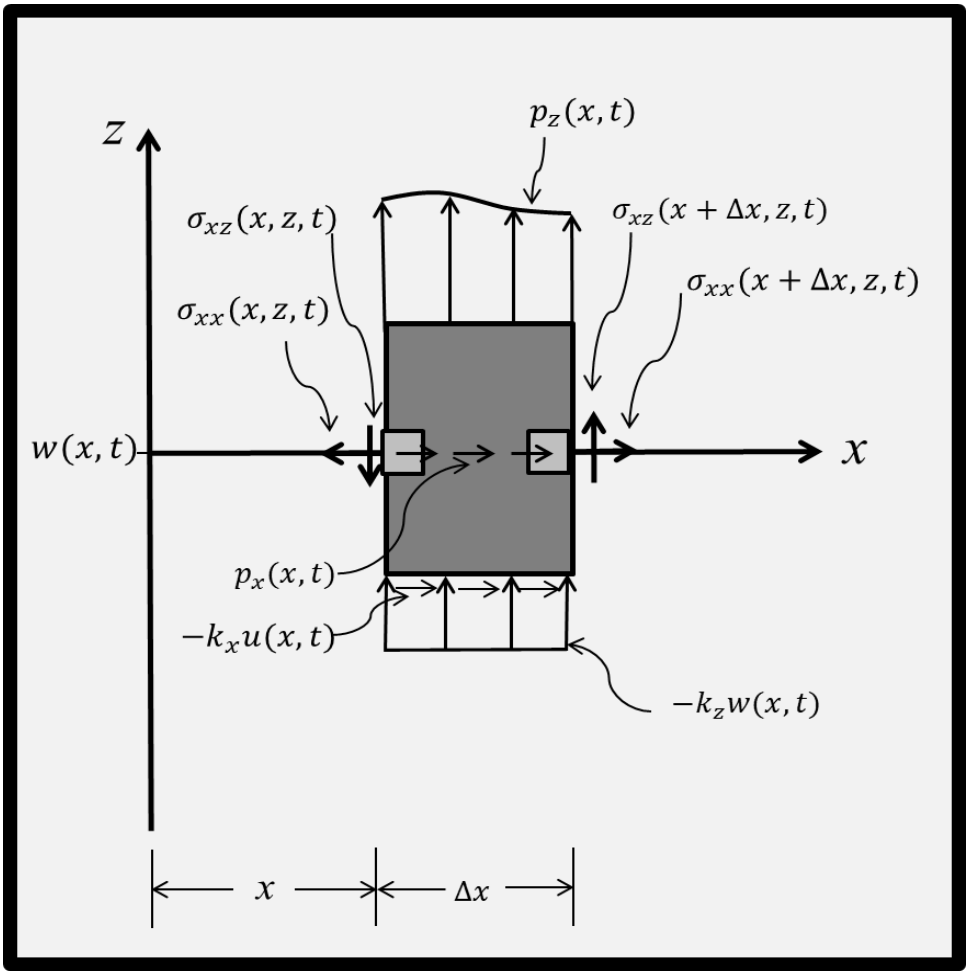

Figure 7 Side View of Free Body Diagram of Cut Rail

Note also that the stress distribution on the two vertical cuts within the rail are denoted generically by the two infinitesimal stress boxes on these faces. Finally, note that the differential element is depicted in the undeformed configuration and it is assumed that the axial force does not affect the vertical displacement of the rail, thus removing the geometric nonlinearity present in the horizontal plane.

Consistent with Euler-Bernoulli beam theory the force and moment resultants in the x-y and x-z planes are now defined as follows (Allen and Haisler 1985):

$$P = P(x,t) \equiv \int_A \sigma_{xx} dA \tag{1}$$

$$V_y = V_y(x,t) \equiv \int_A \sigma_{xy} dA \tag{2}$$

$$V_z = V_z(x,t) \equiv \int_A \sigma_{xz} dA \tag{3}$$

$$M_y = M_y(x,t) \equiv \int_A \sigma_{xx} \bar{z} dA \tag{4}$$

$$M_z = M_z(x,t) \equiv -\int_A \sigma_{xx} \bar{y} dA \tag{5}$$

where A is the cross-sectional area of the rail, $\bar{y}$ is the horizontal distance from the centroid, and $\bar{z}$ is the vertical distance from the centroid. The resultants defined in equations (1)-(5) can be utilized to replace the stress boxes, so that the free body diagrams shown in Fig. 8 and Fig. 9 can be constructed.

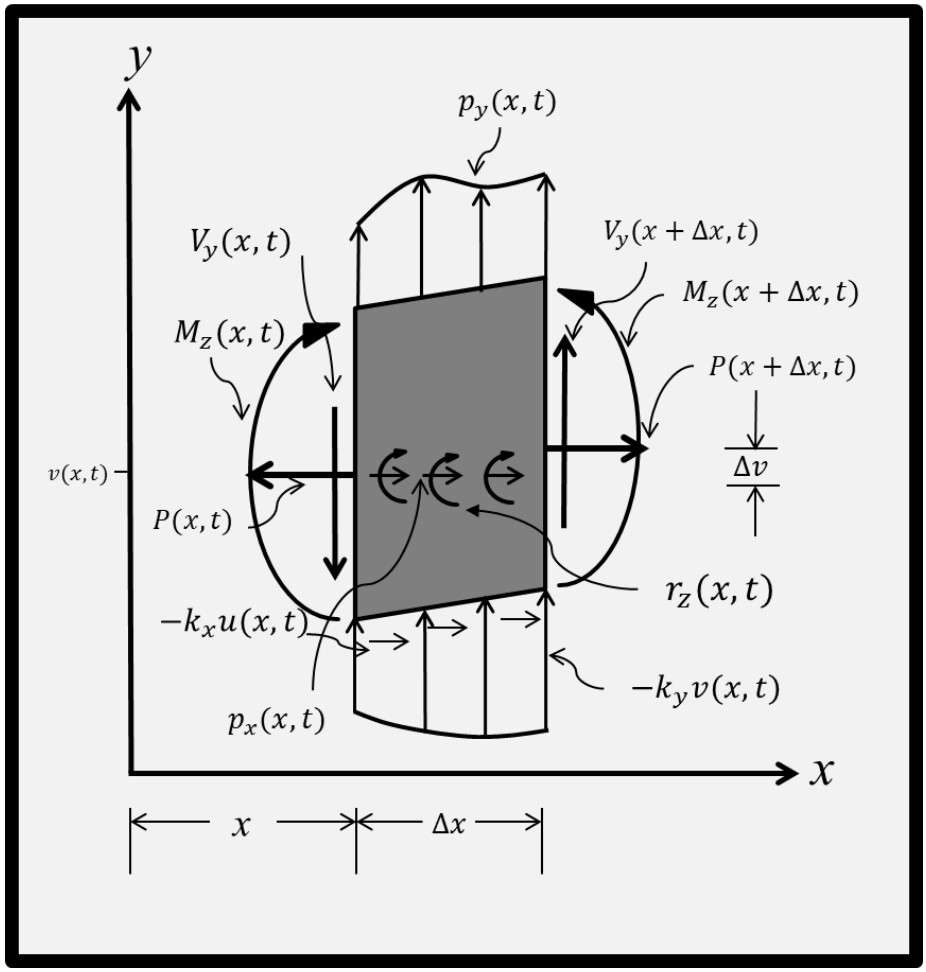

Figure 8 Resultant Forces and Moments Applied to a Differential Element of the Rail in the Horizontal Plane (Reprinted with Permission from Allen and Fry, 2017)

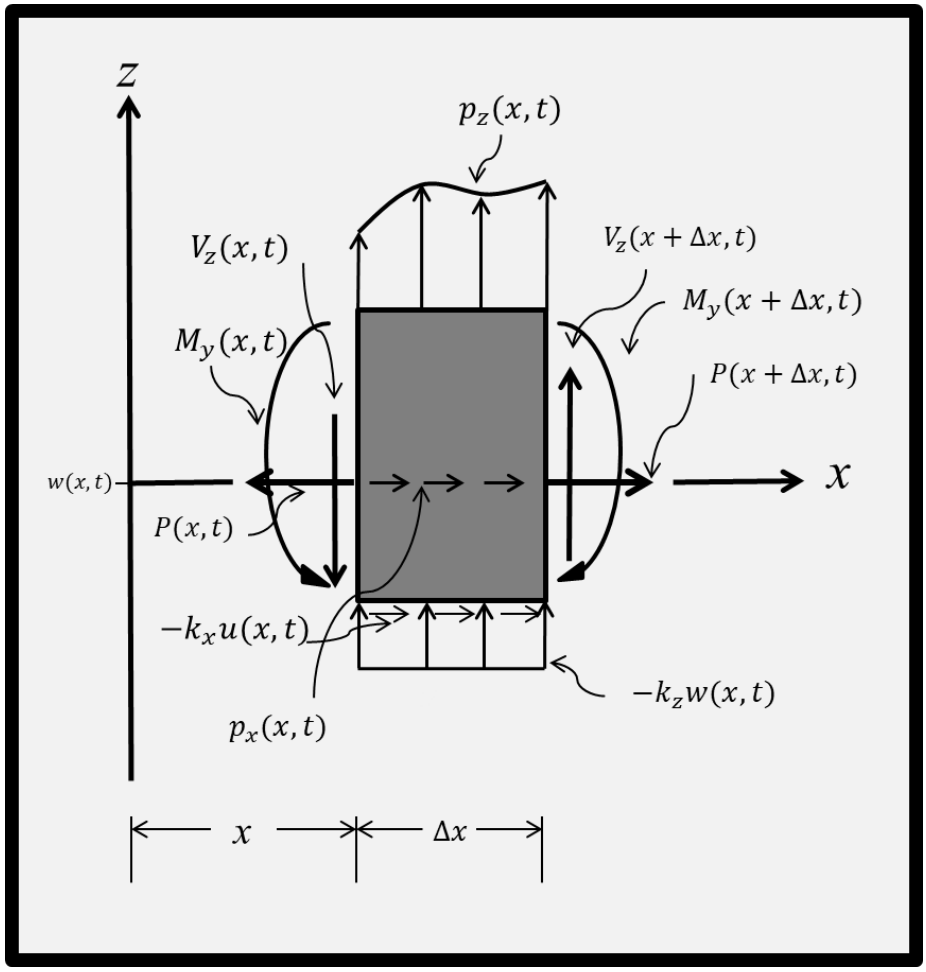

Figure 9 Resultant Forces and Moments Applied to a Differential Element of the Rail in the Vertical Plane

Note that the rotational resistance per unit length, $r_z(x,t)$, has been included in the free body diagram shown in Fig. 8. As illustrated in Fig. 10, this resistance, due to the crosstie and fastener resistance to the rotation of the track, was previously introduced by Grissom and Kerr (Grissom and Kerr 2006). The inclusion of this term is explained by the fact that since the ballast and the fasteners impede rigid-body rotation of the crossties with the track, the crossties apply a moment in the opposite direction from the rotation of the track about the z-axis, and this moment s applied to the rail by the fastener connections.

These moments are therefore pointwise in nature, but are depicted as distributed moments per unit length, $r_z(x,t)$, as a simplification to the model.

This rather ingenious aspect of the model has the advantage that it captures the physical effects of the crossties on the rail response without actually requiring the crossties to be included as structural members, a complicating factor included in at least one more complex model (Lim et al. 2003).

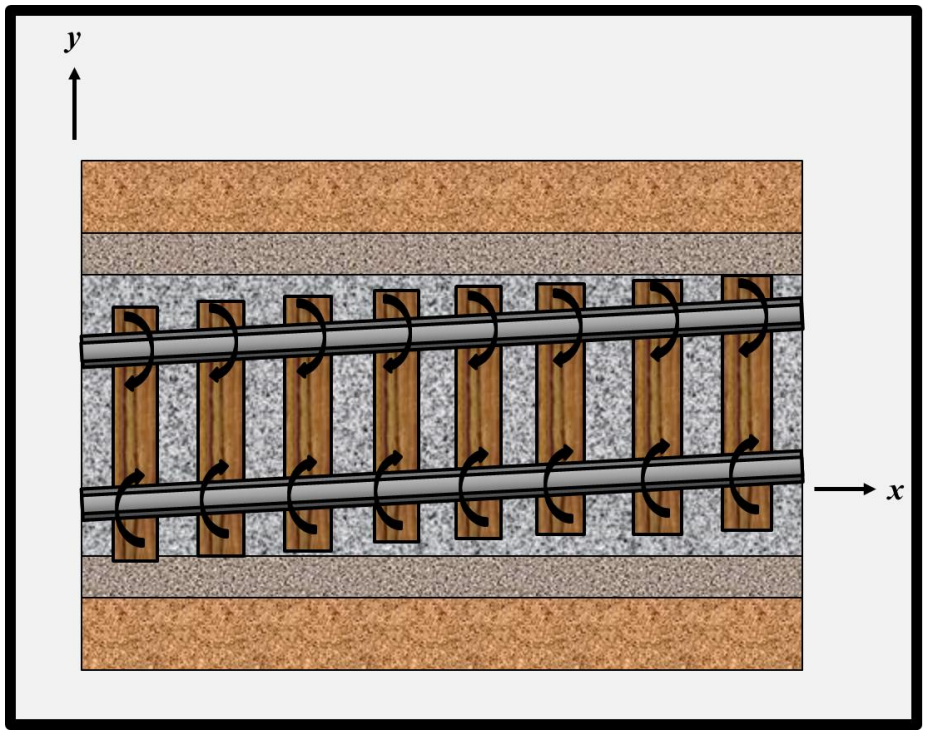

Figure 10 Depiction of the Rotational Resistance of the Fasteners and Crossties (Reprinted with Permission from Allen and Fry, 2017)

Assuming linear thermoelastic behavior, the axial stress within the rail is given by the following constitutive equation:

$$\sigma_{xx} = E(\varepsilon_{xx} - \alpha \Delta T) \tag{6}$$

where is E the modulus of elasticity of the rail, ε_{xx} is the axial strain within the rail, α is the coefficient of thermal expansion within the rail, and ΔT is the temperature change from the rail neutral temperature, which is assumed to be temporally variable, but spatially constant in the current paper. In addition, as shown in Fig. 11 and Fig. 12, the Euler-Bernoulli assumption that plane sections remain plane during the deformations results in the following kinematic relationship (Allen and Haisler 1985):

$$u(x, y) = u(x, 0) - \theta_z(x)\bar{y} + \theta_y(x)\bar{z} \tag{7}$$

where $u(x, 0)$ is the axial displacement of the real neutral surface, which will be denoted throughout the remainder of this paper simply as $u(x)$, $\theta_y = -\frac{dw}{dx}$ is the rotation of the rail neutral surface about the y coordinate axis and $\theta_z = \frac{dv}{dx}$ is the rotation of the rail neutral surface about the z coordinate axis.

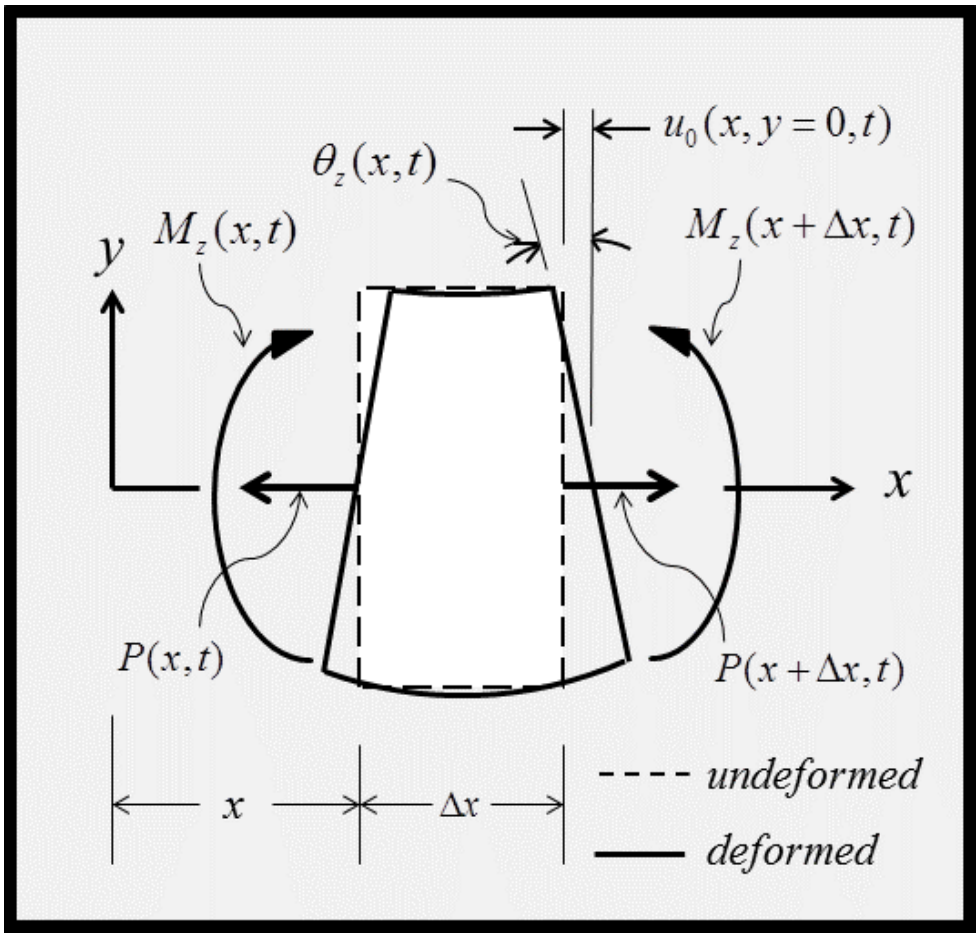

Figure 11 Depiction of the Kinematics of Displacement in an Euler-Bernoulli Beam in the Horizontal Plane (Reprinted with Permission from Allen and Fry, 2017)

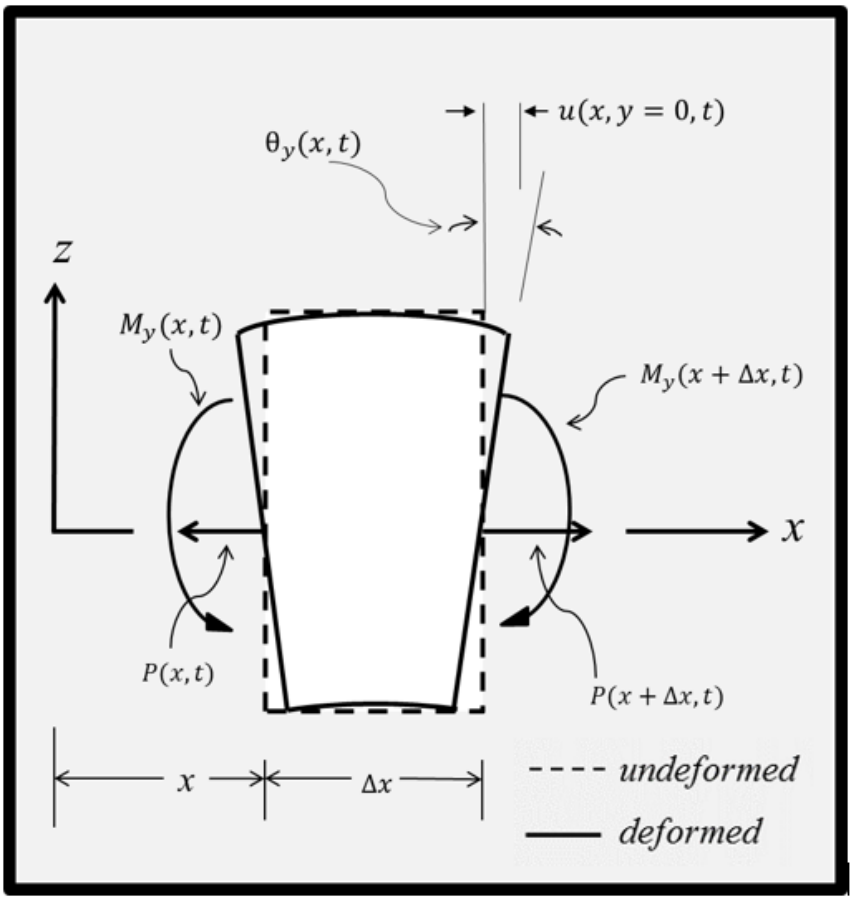

Figure 12 Depiction of the Kinematics of Displacement in an Euler-Bernoulli Beam in the Vertical Plane

Furthermore, the axial strain is approximated by (Tvergaard and Needleman 1981, Grissom and Kerr 2006):

$$\varepsilon_{xx} = \frac{du}{dx} + \frac{1}{2}\left(\frac{dv}{dx}\right)^2 \tag{8}$$

Substituting equation (7) into equation (8), and equation (6) into this result gives the following:

$$\sigma_{xx} = E\left[\frac{du}{dx} - \bar{y}\frac{d\theta_z}{dx} + \bar{z}\frac{d\theta_y}{dx} + \frac{1}{2}\left(\frac{dv}{dx}\right)^2 - \alpha\Delta T\right] \quad (9)$$

In addition, it is assumed that the relation between the rotational stiffness and the track rotation is given by the following constitutive relation:

$$r_z = -S\theta_z \quad (10)$$

Note that in the above equation it is assumed that the relation between the rotation of the track structure about the Z coordinate axis and the angle of rotation is linear (Grissom and Kerr 2006). Whereas limited experimental data support this assumption (Grissom and Kerr 2006), it is to be noted that the rotational stiffness, S, depends strongly on the type of fastener used (Grissom and Kerr 2006).

Furthermore, in the current research it will be assumed that S depends not only on the type of fasteners connecting the track to the crossties, but it is also a weak function of the number of cycles of loading, n_c, previously applied to the truck structure. Thus, at any point in time the relationship described by equation (10) is assumed to apply, but the value of S is at that point in time a constant depending on both the type of fasteners deployed and n_c, thereby quasi-linearizing this effect on the rail response. This assumption is based on anecdotal observation suggesting that the ballast settlement, grinding, spallation and rearrangement over time can affect the rotational resistance of the crosstie-fastener system

to track rotation, and such an assumption will be validated experimentally in future research.

Applying Newton's first law to the forces in the x coordinate direction and moments about the y and z axis in Fig. (8) and (9) together with equations (1)-(10) will result in the general three-dimensional formulation shown in Table 1 for a generic rail subjected to mechanical and spatially constant thermal loading (Kerr 1974, 1978, Allen and Haisler 1985).

Table 1 Model for Predicting the Rail Response

Independent Variables: x, t

Known Inputs:

Loads: $p_x = p_x(x,t),\ p_y = p_y(x,t),\ p_z = p_z(x,t) \quad 0 < x < l$

Temperature change: $\Delta T = \Delta T(t) = known$

Geometry: $A, I_{yy}, I_{zz}, L, \bar{y}, \bar{z}$

Material Properties: $\alpha, E, k_x, k_y, k_z, S$

Unknowns: $u, v, w, \sigma_{xx}, P, V_y, V_z, M_y, M_z$ = **9 unknowns**

Field Equations:

		No. of Equations
(11)	$\frac{dP}{dx} = -p_x + k_x u$	1
(12)	$\frac{dV_y}{dx} = -p_y + k_y v$	1
(13)	$\frac{dV_z}{dx} = -p_z + k_z w$	1
(14)	$\frac{dM_y}{dx} = V_z$	1
(15)	$\frac{dM_z}{dx} = -V_y - (S - P)\frac{dv}{dx}$	1
(16)	$\frac{du}{dx} = \frac{(P+P^T)}{EA} - \frac{1}{2}\left(\frac{dv}{dx}\right)^2$	1
(17)	$\frac{d^2w}{dx^2} = -\frac{M_y}{EI_{yy}}$	1
(18)	$\frac{d^2v}{dx^2} = \frac{M_z}{EI_{zz}}$	1
(19)	$\sigma_{xx} = \frac{(P+P^T)}{A} - \frac{M_z\bar{y}}{I_{zz}} + \frac{M_y\bar{z}}{I_{yy}} - E\alpha\Delta T$	1

Total **9**

where it should be noted that:

x is the coordinate axis in the longitudinal direction of the rail structure

y is the coordinate axis in the horizontal direction of the rail structure

z is the coordinate axis in the vertical direction of the rail structure

$u(x)$ is the displacement of the centroid of the rail in the x coordinate direction

$v(x)$ is the displacement of the centroid of the rail in the y coordinate direction

$w(x)$ is the displacement of the centroid of the rail in the z coordinate direction

$P^T = EA\alpha\Delta T$ is the thermally induced axial force resultant in the x coordinate direction

V_y is the lateral force resultant in the y coordinate direction

V_z is the vertical force resultant in the z coordinate direction

M_y is the resultant moment about the y coordinate axis

M_z is the resultant moment about the z coordinate axis

p_x is the externally applied force per unit length in the x coordinate direction

p_y is the externally applied force per unit length in the y coordinate direction

p_z is the externally applied force per unit length in the z coordinate direction

σ_{xx} is the normal stress component in the x direction

A is twice the cross-sectional area of the rail

I_{yy} is twice the moment of inertia of the rail about the y axis

I_{zz} is twice the moment of inertia of the rail about the z axis

L is the length of the buckled region of the rail

k_x is the x-component of the coefficient of friction of the rail-ballast system

k_y is the y-component of the coefficient of friction of the rail-ballast system

k_z is the z-component of the coefficient of friction (track modulus) of the rail ballast system

E is Young's modulus of the rail

α is the coefficient of thermal expansion of the rail

ΔT is the temperature change of the rail from the rail neutral temperature

It should be apparent that the problem formulated in Table 1 represents a well-posed boundary value problem when appropriate boundary conditions are imposed. However, as there are 9 coupled equations in 9 unknowns, it might be exceedingly difficult to solve, depending on the loading conditions and the material property involved. In particular, the friction coefficients k_x and k_y are observed to be nonlinear, whereas k_z was assumed to behave linearly. Accordingly, although at least one solution has in fact been obtained for specialized conditions (Grissom and Kerr 2006), closed-form solutions are difficult to obtain for this problem. Alternatively, computational solutions are possible using the finite element method, and this approach will be the subject of the next section.

CHAPTER III

VARIATIONAL FORMULATION*

In the present research the displacement components $u(x)$, v(x) and $w(x)$ are treated as primary unknowns. From equation (9) it can be seen that once these are determined the actual stress components follow quite simply, and the remaining unknowns can be calculated using equation (1)-(5). In order to construct a finite element algorithm for predicting the primary unknowns it is first necessary to construct a variational principle in terms of these unknowns. In order to do this, first reduce the term V_y out of the problem by rearranging equation (15) and substituting this result into equation (12), thereby resulting in the following equation:

$$\frac{d}{dx}\left[-\frac{dM_z}{dx}-(S-P)\frac{dv}{dx}\right]=-p_y+k_y v \tag{20}$$

Secondly, reduce the term V_z out of the problem by considering equation (14) and substituting it into equation (12), thereby resulting in the following equation:

$$\frac{d}{dx}\left[\frac{dM_y}{dx}\right]=-p_z+k_z w \tag{21}$$

*Partially reproduced with permission from the authors "Finite Element Formulation and Verification for Thermal Buckling of Rail Structures in the Horizontal Plane" by D Allen and G Fry [2017], CRR Report No. 2017-01

A variational form of equations (11), (20) and (21) may now be constructed by integrating each against an admissible variation in $u(x)$, v(x) and $w(x)$, respectively, thereby resulting in the following variational principle (Reddy 1984):

$$\int_0^L \left[\frac{dP}{dx} + p_x - k_x u\right] \delta u dx + \int_0^L \left[\frac{d}{dx}\left[-\frac{dM_z}{dx} - (S-P)\frac{dv}{dx}\right] + p_y - k_y v\right] \delta v dx + \\ + \int_0^L \left[\frac{d}{dx}\left[\frac{dM_y}{dx}\right] + p_z - k_z w\right] \delta w dx = 0 \qquad (22)$$

where L is an arbitrary longitudinal dimension over which the integration is to be performed and the symbol δ represents an admissible variation in the quantity it precedes. Integrating the differentiated terms in equation (22) by parts results in the following:

$$-\int_0^L P\delta\left(\frac{du}{dx}\right) dx + \int_0^L p_x \delta u \, dx - \int_0^L k_x u \delta u \, dx + [(P\delta u)]_0^L + \\ -\int_0^L \left(-\frac{dM_z}{dx} - (S-P)\frac{dv}{dx}\right) \delta\left(\frac{dv}{dx}\right) dx + \int_0^L p_y \delta v \, dx - \int_0^L k_y v \delta v \, dx + \\ + \left[\left(\left(-\frac{dM_z}{dx} - (S-P)\frac{dv}{dx}\right)\delta v\right)\right]_0^L - \int_0^L \frac{dM_y}{dx}\delta\left(\frac{dw}{dx}\right) dx + \int_0^L p_z \delta w \, dx + \\ - \int_0^L k_z w \delta w \, dx + \left[\left(\frac{dM_y}{dx}\delta w\right)\right]_0^L = 0 \qquad (23)$$

Substituting equations (14), (15), (16) and (18) into equation (23) now results in the following:

$$-\int_0^L \left[EA\frac{du}{dx} - P^T + \frac{EA}{2}\left(\frac{dv}{dx}\right)^2\right]\delta\left(\frac{du}{dx}\right)dx + \int_0^L p_x\delta u\,dx - \int_0^L k_x u\delta u\,dx + [(P\delta u)]_0^L +$$

$$-\int_0^L \frac{d}{dx}\left(EI_{zz}\frac{d^2v}{dx^2}\right)\delta\left(\frac{dv}{dx}\right)dx + \int_0^L \left(S + P^T - EA\frac{du}{dx} - \frac{EA}{2}\left(\frac{dv}{dx}\right)^2\right)\frac{dv}{dx}\delta\left(\frac{dv}{dx}\right)dx +$$

$$+\int_0^L p_y\delta v\,dx - \int_0^L k_y v\delta v\,dx + \left[V_y\delta v\right]_0^L - \int_0^L \frac{d}{dx}\left(EI_{yy}\frac{d^2w}{dx^2}\right)\delta\left(\frac{dw}{dx}\right)dx +$$

$$+\int_0^L p_z\delta w\,dx - \int_0^L k_z w\delta w\,dx + [(V_z\delta w)]_0^L = 0 \qquad (24)$$

Now, integrating by parts the last higher order terms in equation (24) results in the following variational principle:

$$\int_0^L EA\frac{du}{dx}\delta\left(\frac{du}{dx}\right)dx + \int_0^L \left(EI_{zz}\frac{d^2v}{dx^2}\right)\delta\left(\frac{d^2v}{dx^2}\right)dx + \int_0^L \left(EI_{yy}\frac{d^2w}{dx^2}\right)\delta\left(\frac{d^2w}{dx^2}\right)dx +$$

$$-\int_0^L (S + P^T)\frac{dv}{dx}\delta\left(\frac{dv}{dx}\right)dx + \int_0^L EA\frac{du}{dx}\frac{dv}{dx}\delta\left(\frac{dv}{dx}\right)dx + \int_0^L \frac{EA}{2}\left(\frac{dv}{dx}\right)^2\delta\left(\frac{du}{dx}\right)dx +$$

$$+\int_0^L \frac{EA}{2}\left(\frac{dv}{dx}\right)^3\delta\left(\frac{dv}{dx}\right)dx + \int_0^L k_x u\delta u\,dx + \int_0^L k_y v\delta v\,dx + \int_0^L k_z w\delta w\,dx = \int_0^L p_x\delta u\,dx +$$

$$+\int_0^L P^T\,\delta\left(\frac{du}{dx}\right)dx + \int_0^L p_y\delta v\,dx + \int_0^L p_z\delta w\,dx + [(P\delta u)]_0^L + \left[V_y\delta v\right]_0^L +$$

$$+[V_z\delta w]_0^L + \left[M_y\delta\theta_y\right]_0^L + [M_z\delta\theta_z]_0^L \qquad (25)$$

The above is the final form of the variational principle to be implemented within the finite element method.

CHAPTER IV

FINITE ELEMENT FORMULATION*

Equation (25) may now be discretized for a generic frame element. To do this, it is assumed that, within a generic element of length, L_e, the displacement field may be approximated by the following (Reddy 1984, Allen and Haisler 1985):

$$u^e = c_1 + c_2\bar{x}$$
$$v^e = c_3 + c_4\bar{x} + c_5\bar{x}^2 + c_6\bar{x}^3$$
$$w^e = c_7 + c_8\bar{x} + c_9\bar{x}^2 + c_{10}\bar{x}^3 \quad (26)$$

where $\bar{x}$ is the local x coordinate beginning at the left end of element e.

Satisfying boundary conditions at the end points of the local element will result in the following from of equation (26) (Reddy 1984):

$$u^e = \phi_1^e u_1^e + \phi_2^e u_2^e$$
$$v^e = \phi_3^e v_1^e + \phi_4^e \theta_{z1}^e + \phi_5^e v_2^e + \phi_6^e \theta_{z2}^e$$
$$w^e = \phi_7^e w_1^e + \phi_8^e \theta_{y1}^e + \phi_9^e w_2^e + \phi_{10}^e \theta_{y2}^e \quad (27)$$

*Partially reproduced with permission from the authors, "Finite Element Formulation and Verification for Thermal Buckling of Rail Structures in the Horizontal Plane" by D Allen and G Fry [2017], CRR Report No. 2017-01

where u_1^e and u_2^e are the axial displacement components at the left and right ends of element *e*, v_1^e, v_2^e, $w_1^e$and w_2^e are respectively the lateral and vertical displacement components at the left and right ends of element *e*, and θ_{y1}^e, θ_{y2}^e, θ_{z1}^e and θ_{z2}^e are respectively, the rotation components about the y and z axes at the left and right ends of element *e*. The shape functions, ϕ_i^e, are given by (Allen and Haisler 1985, Reddy 2005):

$$\phi_1^e = \left(1 - \frac{\bar{x}}{L_e}\right)$$

$$\phi_2^e = \frac{\bar{x}}{L_e}$$

$$\phi_3^e = 1 - 3\left(\frac{\bar{x}}{L_e}\right)^2 + 2\left(\frac{\bar{x}}{L_e}\right)^3$$

$$\phi_4^e = \bar{x}\left(1 - \frac{\bar{x}}{L_e}\right)^2$$

$$\phi_5^e = 3\left(\frac{\bar{x}}{L_e}\right)^2 - 2\left(\frac{\bar{x}}{L_e}\right)^3$$

$$\phi_6^e = \bar{x}\left[\left(\frac{\bar{x}}{L_e}\right)^2 - \frac{\bar{x}}{L_e}\right]$$

$$\phi_7^e = \phi_3^e = 1 - 3\left(\frac{\bar{x}}{L_e}\right)^2 + 2\left(\frac{\bar{x}}{L_e}\right)^3$$

$$\phi_8^e = -\phi_4^e = -\bar{x}\left(1 - \frac{\bar{x}}{L_e}\right)^2$$

$$\phi_9^e = \phi_5^e = 3\left(\frac{\bar{x}}{L_e}\right)^2 - 2\left(\frac{\bar{x}}{L_e}\right)^3$$

$$\phi_{10}^e = -\phi_6^e = -\bar{x}\left[\left(\frac{\bar{x}}{L_e}\right)^2 - \frac{\bar{x}}{L_e}\right] \tag{28}$$

The assumed displacement field within a generic element represented by equations (27) and (28) may now be substituted into variational principle (25), thereby resulting in algebraic equations of the following form for a generic element (Reddy 1984, Allen and Haisler 1985):

$$\sum_{j=1}^{10} K_{ij}^e\, q_j^e + \sum_{j=1}^{10} B_{ij}^e\, q_j^e + \sum_{j=1}^{10} G_{ij}^e\, q_j^e + \sum_{j=1}^{10} H_{ij}^e\, q_j^e + \sum_{j=1}^{10} M_{ij}^e\, q_j^e + \sum_{j=1}^{10} N_{ij}^e\, q_j^e = F_i^e$$

$$i = 1, \ldots 10 \tag{29}$$

where each term above accounts for one or more terms in equation (25), as shown below in equations (30)-(36):

$$\left[K_{ij}^e\right] = \int_0^L EA\frac{du}{dx}\delta\left(\frac{du}{dx}\right)dx + \int_0^L \left(EI_{zz}\frac{d^2v}{dx^2}\right)\delta\left(\frac{d^2v}{dx^2}\right)dx + \int_0^L \left(EI_{yy}\frac{d^2w}{dx^2}\right)\delta\left(\frac{d^2w}{dx^2}\right)dx \tag{30}$$

$$\left[B_{ij}^e\right] = -\int_0^L (S + P^T)\frac{dv}{dx}\delta\left(\frac{dv}{dx}\right)dx \tag{31}$$

$$\left[G_{ij}^e\right] = \int_0^L EA\frac{du}{dx}\frac{dv}{dx}\delta\left(\frac{dv}{dx}\right)dx \tag{32}$$

$$\left[H_{ij}^e\right] = \int_0^L \frac{EA}{2}\left(\frac{dv}{dx}\right)^2\delta\left(\frac{du}{dx}\right)dx \tag{33}$$

$$\left[M_{ij}^e\right] = \int_0^L \frac{EA}{2}\left(\frac{dv}{dx}\right)^3\delta\left(\frac{dv}{dx}\right)dx \tag{34}$$

$$\left[N_{ij}^e\right] = \int_0^L k_x u\delta u\,dx + \int_0^L k_y v\delta v\,dx + \int_0^L k_z w\delta w\,dx \tag{35}$$

$$\left[F_{ij}^{e}\right] = \int_0^L p_x \delta u \, dx + \int_0^L P^T \, \delta \left(\frac{du}{dx}\right) dx + \int_0^L p_y \delta v \, dx + \int_0^L p_z \delta w \, dx \tag{36}$$

Furthermore, note that nonlinear matrices H_{ij}^{e} and M_{ij}^{e} presented in equations (33) and (34) will be neglected in the implementation of this model under the assumption that linear small strain theory is sufficient to accurately predict lateral thermal buckling in rails. In addition,

$$\left\{q_j^e\right\} \equiv \begin{Bmatrix} u_1^e \\ v_1^e \\ w_1^e \\ \theta_{y1}^e \\ \theta_{z1}^e \\ u_2^e \\ v_2^e \\ w_2^e \\ \theta_{y2}^e \\ \theta_{z2}^e \end{Bmatrix} \tag{37}$$

And,

$$[K^e] = \begin{bmatrix} \frac{E^eA^e}{L^e} & 0 & 0 & 0 & 0 & -\frac{E^eA^e}{L^e} & 0 & 0 & 0 & 0 \\ 0 & \frac{12E^eI^e_{zz}}{(L^e)^3} & 0 & 0 & \frac{6E^eI^e_{zz}}{(L^e)^2} & 0 & -\frac{12E^eI^e_{zz}}{(L^e)^3} & 0 & 0 & \frac{6E^eI^e_{zz}}{(L^e)^2} \\ 0 & 0 & \frac{12E^eI^e_{yy}}{(L^e)^3} & -\frac{6E^eI^e_{yy}}{(L^e)^2} & 0 & 0 & 0 & -\frac{12E^eI^e_{yy}}{(L^e)^3} & -\frac{6E^eI^e_{yy}}{(L^e)^2} & 0 \\ 0 & 0 & -\frac{6E^eI^e_{yy}}{(L^e)^2} & \frac{4E^eI^e_{yy}}{L^e} & 0 & 0 & 0 & \frac{6E^eI^e_{yy}}{(L^e)^2} & \frac{2E^eI^e_{yy}}{L^e} & 0 \\ 0 & \frac{6E^eI^e_{zz}}{(L^e)^2} & 0 & 0 & \frac{4E^eI^e_{yy}}{L^e} & 0 & -\frac{6E^eI^e_{zz}}{(L^e)^2} & 0 & 0 & \frac{2E^eI^e_{zz}}{L^e} \\ -\frac{E^eA^e}{L^e} & 0 & 0 & 0 & 0 & \frac{E^eA^e}{L^e} & 0 & 0 & 0 & 0 \\ 0 & -\frac{12E^eI^e_{zz}}{(L^e)^3} & 0 & 0 & -\frac{6E^eI^e_{zz}}{(L^e)^2} & 0 & \frac{12E^eI^e_{zz}}{(L^e)^3} & 0 & 0 & -\frac{6E^eI^e_{zz}}{(L^e)^2} \\ 0 & 0 & -\frac{12E^eI^e_{yy}}{(L^e)^3} & \frac{6E^eI^e_{yy}}{(L^e)^2} & 0 & 0 & 0 & \frac{12E^eI^e_{yy}}{(L^e)^3} & \frac{6E^eI^e_{yy}}{(L^e)^2} & 0 \\ 0 & 0 & -\frac{6E^eI^e_{yy}}{(L^e)^2} & \frac{2E^eI^e_{yy}}{L^e} & 0 & 0 & 0 & \frac{6E^eI^e_{yy}}{(L^e)^2} & \frac{4E^eI^e_{yy}}{L^e} & 0 \\ 0 & \frac{6E^eI^e_{zz}}{(L^e)^2} & 0 & 0 & \frac{2E^eI^e_{zz}}{L^e} & 0 & -\frac{6E^eI^e_{zz}}{(L^e)^2} & 0 & 0 & \frac{4E^eI^e_{zz}}{L^e} \end{bmatrix} \tag{38}$$

Furthermore, for linearly varying distributed lateral and vertical loads given by:

$$p_y(\bar{x}) = p_y^0 + (p_y^{L^e} - p_y^0)\frac{\bar{x}}{L^e}$$

$$p_z(\bar{x}) = p_z^0 + (p_z^{L^e} - p_z^0)\frac{\bar{x}}{L^e} \tag{39}$$

$$\{F^e\} = \begin{Bmatrix} \frac{p_x L^e}{2} - E^e A^e \alpha^e \Delta T^e \\ \frac{p_y^0 L^e}{2} + \frac{3L^e}{20}\left(p_y^{L^e} - p_y^0\right) \\ \frac{p_z^0 L^e}{2} + \frac{3L^e}{20}\left(p_z^{L^e} - p_z^0\right) \\ -\frac{p_z^0 (L^e)^2}{12} - \frac{(L^e)^2}{30}\left(p_z^{L^e} - p_z^0\right) \\ \frac{p_y^0 (L^e)^2}{12} + \frac{(L^e)^2}{30}\left(p_y^{L^e} - p_y^0\right) \\ \frac{p_x L^e}{2} + E^e A^e \alpha^e \Delta T^e \\ \frac{p_y^0 L^e}{2} + \frac{7L^e}{20}\left(p_y^{L^e} - p_y^0\right) \\ \frac{p_z^0 L^e}{2} + \frac{7L^e}{20}\left(p_z^{L^e} - p_z^0\right) \\ \frac{p_z^0 (L^e)^2}{12} + \frac{(L^e)^2}{20}\left(p_z^{L^e} - p_z^0\right) \\ -\frac{p_y^0 (L^e)^2}{12} - \frac{(L^e)^2}{20}\left(p_y^{L^e} - p_y^0\right) \end{Bmatrix} \quad (40)$$

Note that the boundary terms are not included because they will cancel one another when the global equations are assembled.

When equations (31)-(36) might be neglected, the standard finite element formulation for a linear thermoelastic beam undergoing small displacements is recovered. However, in the current case it remains to account for all the terms presented in equation (25) or (31)-(36).

Consider first the fourth term in equation (25), which corresponds to the right-hand side of equation (31). This term is given by:

$$\{B^e\} = -(S + P^T)\begin{bmatrix} 0 & 0 & 0 & 0 & 0 & 0 & 0 & 0 & 0 & 0 \\ 0 & \frac{6}{5L^e} & 0 & 0 & 0.10 & 0 & -\frac{6}{5L^e} & 0 & 0 & 0.10 \\ 0 & 0 & 0 & 0 & 0 & 0 & 0 & 0 & 0 & 0 \\ 0 & 0 & 0 & 0 & 0 & 0 & 0 & 0 & 0 & 0 \\ 0 & 0.10 & 0 & 0 & \frac{2L^e}{15} & 0 & -0.10 & 0 & 0 & -\frac{L^e}{30} \\ 0 & 0 & 0 & 0 & 0 & 0 & 0 & 0 & 0 & 0 \\ 0 & -\frac{6}{5L^e} & 0 & 0 & -0.10 & 0 & \frac{6}{5L^e} & 0 & 0 & -0.10 \\ 0 & 0 & 0 & 0 & 0 & 0 & 0 & 0 & 0 & 0 \\ 0 & 0 & 0 & 0 & 0 & 0 & 0 & 0 & 0 & 0 \\ 0 & 0.10 & 0 & 0 & -\frac{L^e}{30} & 0 & -0.10 & 0 & 0 & \frac{2L^e}{15} \end{bmatrix} \quad (41)$$

Now consider the fifth term in equation (25), which corresponds to the right-hand side of equation (32). This term in nonlinear, being first order in both $u(x)$ and $v(x)$ at any point in time. In the case wherein it is sufficiently accurate to assume that $u(x, t + \Delta t)$ may be approximated by the values of the previous step, $u(x, t)$, the result is as follows:

$$\{G^e(t + \Delta t)\} = EA\left(\frac{u_2^e(t) - u_1^e(t)}{L^e}\right)\begin{bmatrix} 0 & 0 & 0 & 0 & 0 & 0 & 0 & 0 & 0 & 0 \\ 0 & \frac{6}{5L^e} & 0 & 0 & 0.10 & 0 & -\frac{6}{5L^e} & 0 & 0 & 0.10 \\ 0 & 0 & 0 & 0 & 0 & 0 & 0 & 0 & 0 & 0 \\ 0 & 0 & 0 & 0 & 0 & 0 & 0 & 0 & 0 & 0 \\ 0 & 0.10 & 0 & 0 & \frac{2L^e}{15} & 0 & -0.10 & 0 & 0 & -\frac{L^e}{30} \\ 0 & 0 & 0 & 0 & 0 & 0 & 0 & 0 & 0 & 0 \\ 0 & -\frac{6}{5L^e} & 0 & 0 & -0.10 & 0 & \frac{6}{5L^e} & 0 & 0 & -0.10 \\ 0 & 0 & 0 & 0 & 0 & 0 & 0 & 0 & 0 & 0 \\ 0 & 0 & 0 & 0 & 0 & 0 & 0 & 0 & 0 & 0 \\ 0 & 0.10 & 0 & 0 & -\frac{L^e}{30} & 0 & -0.10 & 0 & 0 & \frac{2L^e}{15} \end{bmatrix} \quad (42)$$

Now consider the eighth, ninth and tenth terms in equation (25), which correspond to equation (35). In the case wherein it is sufficiently accurate to assume that the coefficients of friction, k_x and k_y vary linearly in x in each element, the result is as follows:

$$[N^e] = \begin{bmatrix} A & B \\ C & D \end{bmatrix} \tag{43}$$

Where

$[A] =$

$$\begin{bmatrix} \frac{k_x^L L_e}{3} + \frac{(k_x^R - k_x^L)L_e}{12} & 0 & 0 & 0 & 0 \\ 0 & \frac{13k_y^L L_e}{35} + \frac{3(k_y^R - k_y^L)L_e}{35} & 0 & 0 & \frac{11k_y^L (L_e)^2}{210} + \frac{(k_y^R - k_y^L)(L_e)^2}{60} \\ 0 & 0 & \frac{13k_z L_e}{35} & -\frac{11k_z (L_e)^2}{210} & 0 \\ 0 & 0 & -\frac{11k_z (L_e)^2}{210} & \frac{k_z (L_e)^3}{105} & 0 \\ 0 & \frac{11k_y^L (L_e)^2}{210} + \frac{(k_y^R - k_y^L)(L_e)^2}{60} & 0 & 0 & \frac{k_y^L (L_e)^3}{105} + \frac{(k_y^R - k_y^L)(L_e)^3}{280} \end{bmatrix}$$

$[B] =$

$$\begin{bmatrix} \frac{k_x^L L_e}{6} + \frac{(k_x^R - k_x^L)L_e}{12} & 0 & 0 & 0 & 0 \\ 0 & \frac{9k_y^L L_e}{70} + \frac{9(k_y^R - k_y^L)L_e}{140} & 0 & 0 & -\frac{13k_y^L (L_e)^2}{420} - \frac{(k_y^R - k_y^L)(L_e)^2}{70} \\ 0 & 0 & \frac{9k_z L_e}{70} & \frac{13k_z (L_e)^2}{420} & 0 \\ 0 & 0 & \frac{13k_z (L_e)^2}{420} & -\frac{k_z (L_e)^3}{140} & 0 \\ 0 & \frac{13k_y^L (L_e)^2}{420} + \frac{(k_y^R - k_y^L)(L_e)^2}{60} & 0 & 0 & -\frac{k_y^L (L_e)^3}{140} - \frac{(k_y^R - k_y^L)(L_e)^3}{280} \end{bmatrix}$$

$$[C] =$$

$$\begin{bmatrix} \frac{k_x^L L_e}{6} + \frac{(k_x^R - k_x^L)L_e}{12} & 0 & 0 & 0 & 0 \\ 0 & \frac{9k_y^L L_e}{70} + \frac{9(k_y^R - k_y^L)L_e}{140} & 0 & 0 & \frac{13k_y^L (L_e)^2}{420} + \frac{(k_y^R - k_y^L)(L_e)^2}{60} \\ 0 & 0 & \frac{9k_z L_e}{70} & -\frac{13k_z (L_e)^2}{420} & 0 \\ 0 & 0 & -\frac{13k_z (L_e)^2}{420} & \frac{k_z (L_e)^3}{140} & 0 \\ 0 & -\frac{13k_y^L (L_e)^2}{420} - \frac{(k_y^R - k_y^L)(L_e)^2}{70} & 0 & 0 & -\frac{k_y^L (L_e)^3}{140} - \frac{(k_y^R - k_y^L)(L_e)^3}{280} \end{bmatrix}$$

$$[D] =$$

$$\begin{bmatrix} \frac{k_x^L L_e}{3} + \frac{(k_x^R - k_x^L)L_e}{4} & 0 & 0 & 0 & 0 \\ 0 & \frac{13k_y^L L_e}{35} + \frac{2(k_y^R - k_y^L)L_e}{7} & 0 & 0 & -\frac{11k_y^L (L_e)^2}{210} - \frac{(k_y^R - k_y^L)(L_e)^2}{28} \\ 0 & 0 & \frac{13k_z L_e}{35} & \frac{11k_z (L_e)^2}{210} & 0 \\ 0 & 0 & \frac{11k_z (L_e)^2}{210} & \frac{k_z (L_e)^3}{105} & 0 \\ 0 & -\frac{11k_y^L (L_e)^2}{210} - \frac{(k_y^R - k_y^L)(L_e)^2}{28} & 0 & 0 & \frac{k_y^L (L_e)^3}{105} + \frac{(k_y^R - k_y^L)(L_e)^3}{168} \end{bmatrix}$$

and

$$k_x(x) = k_x^L + (k_x^R - k_x^L)\frac{x}{L_e}$$

$$k_y(x) = k_y^L + (k_y^R - k_y^L)\frac{x}{L_e}$$

$$k_z(x) = k_z = const. \qquad (44)$$

where in addition $k_{x,y}^{L}$ and $k_{x,y}^{R}$ are the values of the axial and lateral coefficients of friction at $x = 0, L_e$ within the element and k_z is the vertical coefficient of friction (or track modulus) within the element.

The above element equations may be assembled into a global finite element formulation using the standard assembly technique, and this has been accomplished by the authors. This then completes the finite element formulation.

CHAPTER V

VALIDATION OF THE FINITE ELEMENT ALGORITHM*

The following sections will present several example problems for the purpose of validating the finite element algorithm developed herein.

Validation Problems for the Linear Case

The finite element algorithm is now validated for the linear case ($k_y = k_y^0 =$ constant) with the following example problems. Note that the AREMA 115L-10 rail head section was chosen arbitrarily to represent a generic rail of typical dimensions. Therefore, its material and geometric properties were utilized throughout this report in accordance with industry specifications (Nippon Steel Corporation 2020) such that the response of a realistic rail section could be modeled.

Example Problem #1

Given: A double-cantilevered beam is subjected to an evenly distributed transverse loading $p_y = p_y^0 = 10^4 N/m$. In addition, E=2.06x10^{11} *N/m*^{2}, I_{zz}=8.99x10^{-6} *m*^{4}, $p_x = k_x = k_y = S = 0$ and l=12 *m.*

Required: a) Solve for $v = v(x, p_y^0, E, I_{zz})$ analytically

b) Obtain a solution for $v = v(x, p_y^0, E, I_{zz})$ using the finite element method and compare the two solutions

*Partially reproduced with permission from the authors, "Finite Element Formulation and Verification for Thermal Buckling of Rail Structures in the Horizontal Plane" by D Allen and G Fry [2017], CRR Report No. 2017-01

Solution: a) For this case ($\Delta T = k_y = 0$) the formulation simplifies to the following:

$$\frac{d^2}{dx^2}\left(EI_{zz}\frac{d^2v}{dx^2}\right) = p_y^0 \tag{E1.1}$$

Now integrate equation (E1.1) to obtain:

$$\frac{d}{dx}\left(EI_{zz}\frac{d^2v}{dx^2}\right) = p_y^0 x + c_1 \tag{E1.2}$$

where c_1 is a constant of integration. Integrating a second time gives:

$$EI_{zz}\frac{d^2v}{dx^2} = p_y^0\frac{x^2}{2} + c_1 x + c_2 \tag{E1.3}$$

where c_2 is a constant of integration. Integrating a third time gives:

$$\frac{dv}{dx} = \frac{1}{EI_{zz}}\left[p_y^0\frac{x^3}{6} + c_1\frac{x^2}{2} + c_2 x + c_3\right] \tag{E1.4}$$

where c_3 is a constant of integration. Integrating a fourth time gives:

$$v = \frac{1}{EI_{zz}}\left[p_y^0\frac{x^4}{24} + c_1\frac{x^3}{6} + c_2\frac{x^2}{2} + c_3 x + c_4\right] \tag{E1.5}$$

Next apply the following boundary condition:

$$v(x = 0) = 0 \Rightarrow c_4 = 0 \tag{E1.6}$$

Next apply the following boundary condition:

$$\frac{dv}{dx}(x = 0) = 0 \Rightarrow c_3 = 0 \tag{E1.7}$$

Substituting equations (E1.6) and (E1.7) into equation (E1.5) results in the following:

$$v = \frac{1}{EI_{zz}}\left[p_y^0 \frac{x^4}{24} + c_1 \frac{x^3}{6} + c_2 \frac{x^2}{2}\right] \tag{E1.8}$$

Next apply the following boundary condition:

$$v(x = l) = 0 \Rightarrow 0 = p_y^0 \frac{l^4}{24} + c_1 \frac{l^3}{6} + c_2 \frac{l^2}{2} \tag{E1.9}$$

Now apply the final boundary condition:

$$\frac{dv}{dx}(x = l) = 0 \Rightarrow 0 = p_y^0 \frac{l^3}{6} + c_1 \frac{l^2}{2} + c_2 l \tag{E1.10}$$

Equations (E1.9) and (E1.10) are two equations in the two unknown coefficients c_1 and c_2. Solving for these two unknowns results in the following:

$$c_1 = -p_y^0 \frac{l}{2} \quad c_2 = p_y^0 \frac{l^2}{12} \tag{E1.11}$$

Substituting (E1.11) into (E1.8) therefore results in the following exact solution:

$$v = \frac{p_y^0}{EI_{zz}} \left[\frac{x^4}{24} - \frac{l}{12} x^3 + \frac{l^2}{24} x^2 \right] \tag{E1.12}$$

In addition, substituting (E6) and (E10) into (E3) results in:

$$\frac{dv}{dx} = \frac{p_y^0}{EI_{zz}} \left[\frac{x^3}{6} - \frac{l}{4} x^2 + \frac{l^2}{12} x \right] \tag{E1.13}$$

b) The finite element algorithm is now deployed using 6 elements of equal length. Comparative results are shown in Fig. 13.

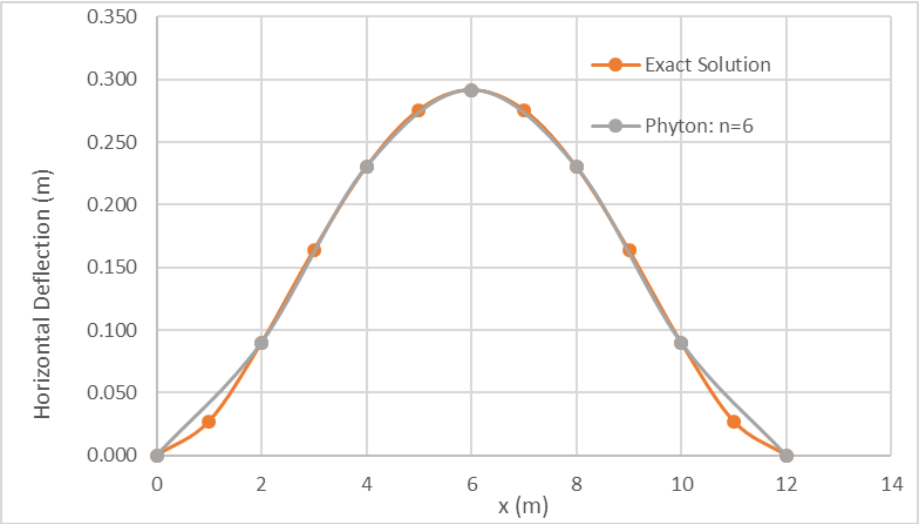

Figure 13 Comparison of Computational Result to Exact Solution for Example Problem #1 in the Horizontal Plane

Note that by following the procedure shown in part a) it is possible to obtain an equivalent exact solution for the vertical displacement in the x-z plane, which results in the following:

$$w = \frac{p_z^0}{EI_{yy}}\left[\frac{x^4}{24} - \frac{l}{12}x^3 + \frac{l^2}{24}x^2\right] \qquad \text{(E1.14)}$$

The finite element algorithm is now deployed using six elements of equal length and setting $I_{yy} = I_{zz}$ and $p_z^0 = p_y^0$. Comparative results are shown in Fig. 14.

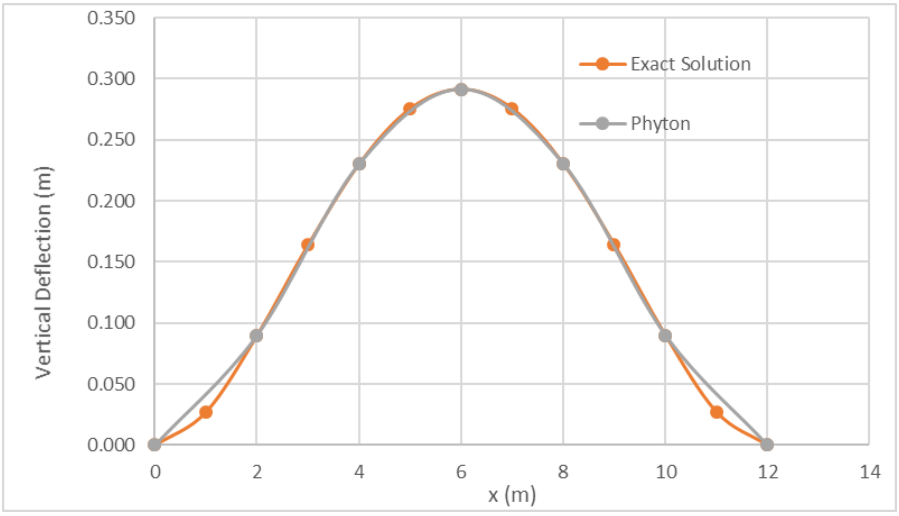

Figure 14 Comparison of Computational Result to Exact Solution for Example Problem #1 in the Vertical Plane

As expected, the vertical and horizontal displacements are equivalent for equal loads, geometry, and material properties.

Example Problem #2

Given: A cantilevered beam is subjected to the triangular distributed transverse loading shown in Fig. 15 with $p_y = p_y^0 = 10^4 N/m$. In addition, E=2.06x10^{11} N/m^2, I_{zz}=8.99x10^{-6} m^4, $p_x = k_x = k_y = S = 0$ and l=12 m.

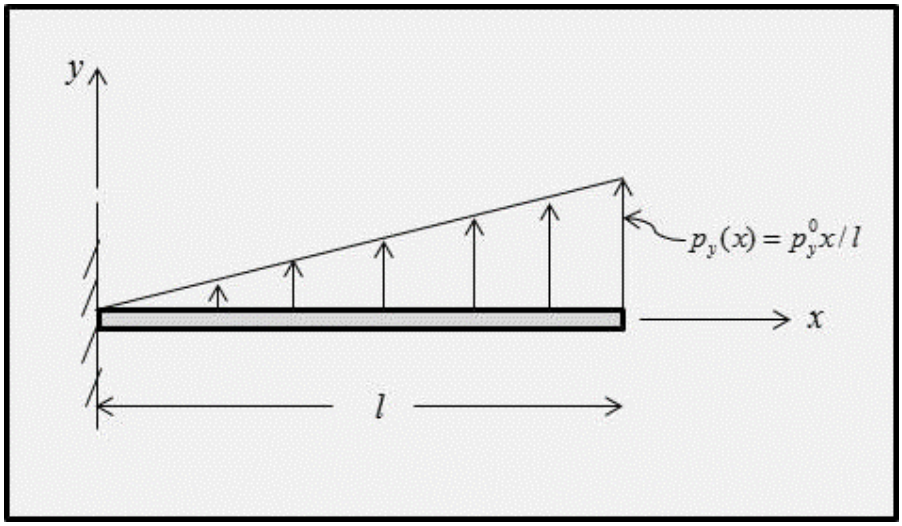

Figure 15 Depiction of a Prismatic Cantilever Beam Subjected to Transverse Triangular Loading (Reprinted with Permission from Allen and Fry, 2017)

Required: a) Solve for $v = v(x, p_y^0, E, I_{yy})$ analytically

b) Obtain a solution for v= $v(x, p_y^0, E, I_{zz})$ numerically and compare the two solutions

Solution: a) To obtain the analytic solution to this problem, first note that

$$p_y(x) = p_y^l \frac{x}{l} \tag{E2.1}$$

Now recall that the beam shear, $V_z(x)$, is given by the following:

$$\frac{dV_y}{dx} = -p_y \tag{E2.2}$$

Therefore, substituting (E2.1) into (E2.2) and integrating results in the following:

$$\int \frac{dV_y}{dx} dx = -\int p_y^l \frac{x}{l} dx \Rightarrow V_y(x) = -p_y^l \frac{x^2}{2l} + c_1 \quad \text{(E2.3)}$$

Now consider the following boundary condition:

$$V_y(x = l) = 0 \quad \text{(E2.4)}$$

Substituting (E2.4) into (E2.3) gives the following:

$$c_1 = \frac{p_y^l l}{2} \Rightarrow V_y(x) = -\frac{p_y^l}{2l}(x^2 - l^2) \quad \text{(E2.5)}$$

Now recall the beam moment, $M_z(x)$, is given by the following:

$$\frac{dM_z}{dx} = -V_y \quad \text{(E2.6)}$$

Therefore, substituting (E2.5) into (E2.6) results in the following:

$$\frac{dM_z}{dx} = \frac{p_y^l}{2l}(x^2 - l^2) \quad \text{(E2.7)}$$

Integrating equation (E2.7) therefore gives the following:

$$M_z(x) = \frac{p_y^l}{2l}\left(\frac{x^3}{3} - l^2 x\right) + c_2 \tag{E2.8}$$

Now consider the following boundary condition:

$$M_z(x = l) = 0 \tag{E2.9}$$

Substituting (E2.9) into (E2.8) gives the following:

$$c_2 = \frac{p_y^l l^2}{3} \Rightarrow M_z(x) = \frac{p_y^l}{2l}\left(\frac{x^3}{3} - l^2 x + \frac{2l^3}{3}\right) \tag{E2.10}$$

Now consider the following equation:

$$\frac{d^2 v}{dx^2} = \frac{M_z}{EI_{zz}} \tag{E2.11}$$

Substituting (E2.10) into (E2.11) thus results in:

$$\frac{d^2 v}{dx^2} = \frac{p_y^l}{2lEI_{zz}}\left(\frac{x^3}{3} - l^2 x + \frac{2l^3}{3}\right) \tag{E2.12}$$

Integrating the above thus gives:

$$\theta_z(x) = \frac{dv}{dx} = \frac{p_y^l}{2lEI_{zz}}\left(\frac{x^4}{12} - \frac{l^2x^2}{2} + \frac{2l^3x}{3}\right) + c_3 \quad \text{(E2.13)}$$

Now consider the following boundary condition:

$$\theta_z(x = 0) = 0 \quad \text{(E2.14)}$$

Substituting (E2.14) into (E2.13) gives the following:

$$c_3 = 0 \Rightarrow \theta_z(x) = \frac{p_y^l}{2lEI_{zz}}\left(\frac{x^4}{12} - \frac{l^2x^2}{2} + \frac{2l^3x}{3}\right) \quad \text{(E2.15)}$$

It follows that:

$$\theta_z(x = l) = \frac{p_y^l l^3}{4EI_{zz}} \quad \text{(E2.16)}$$

Integrating equation (E.15) gives the following:

$$v(x) = \frac{p_y^l}{2lEI_{zz}}\left(\frac{x^5}{60} - \frac{l^2x^3}{6} + \frac{l^3x^2}{3}\right) + c_4 \quad \text{(E2.17)}$$

Now consider the following boundary condition:

$$v(x=0)=0 \tag{E2.18}$$

Substituting (E2.18) into (E2.17) results in the following:

$$c_4=0 \Rightarrow v(x)=\frac{p_y^l}{2lEI_{zz}}\left(\frac{x^5}{60}-\frac{l^2x^3}{6}+\frac{l^3x^2}{3}\right) \tag{E2.19}$$

It follows that

$$v(x=l)=\frac{11p_y^l l^4}{120EI_{zz}} \tag{E2.20}$$

a) The finite element solution is obtained using 6 elements of equal length. Comparative results are shown in Fig. 16.

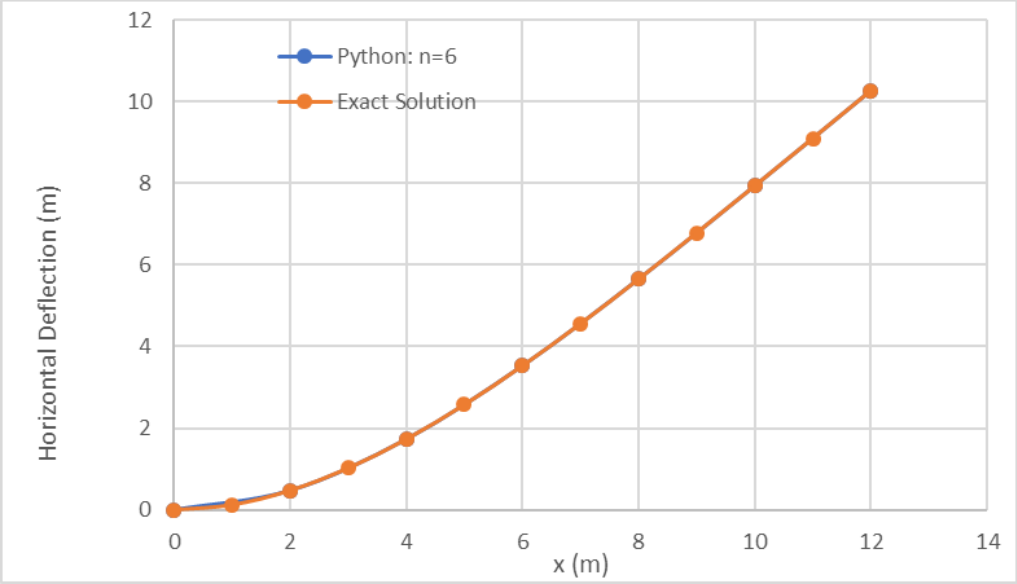

Figure 16 Comparison of Computational Result to Exact Solution for Example Problem #2 in the Horizontal Plane

Note that by following the procedure shown in part a) it is possible to obtain an equivalent exact solution for the vertical displacement in the x-z plane, which results in the following:

$$w(x) = \frac{p_z^l}{2lEI_{yy}}\left(\frac{x^5}{60} - \frac{l^2x^3}{6} + \frac{l^3x^2}{3}\right) \qquad \text{(E2.21)}$$

The finite element algorithm is now deployed using six elements of equal length and setting $I_{yy} = I_{zz}$ and $p_z^0 = p_y^0$. Comparative results are shown in Fig. 17.

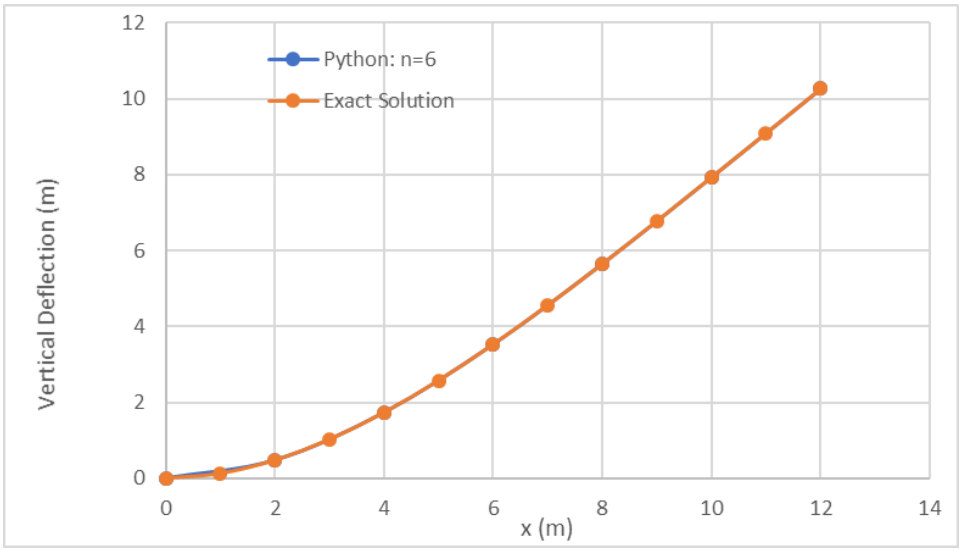

Figure 17 Comparison of Computational Result to Exact Solution for Example Problem #2 in the Vertical Plane

As expected, the vertical and horizontal displacements are equivalent for equal loads, geometry, and material properties.

Example Problem #3

Given: A simply supported beam is subjected to a temperature change of $\Delta T = 50\ °C$. Properties are E=2.06x10^{11} N/m^2, I_{zz}=8.99x10^{-6} m^4, A=0.0145 m^2, $p_x = k_x = k_y = S = 0$, l=12.0 m and $\alpha = 1.05x10^{-5}\ /°C$.

Required: a) Find a form of $p_y = p_y(x)$ that provides an analytic solution for

$$v = v(x, p_y^0, E, I_{zz})$$

b) obtain a solution using finite elements and compare the two

Solution: a) The solution solves the following differential equation:

$$EI_{zz}\frac{d^4v}{dx^4} + P^T\frac{d^2v}{dx^2} = p_y \qquad \text{(E3.1)}$$

In order to obtain an analytic solution, assume that the solution is of the form:

$$v(x) = a_0 + a_1x + a_2x^2 + a_3x^3 + a_4x^4 \qquad \text{(E3.2)}$$

Next, consider the boundary conditions:

$$\text{at x=0, } l\text{: } v = 0,\ \frac{d^2v}{dx^2} = 0 \qquad \text{(E3.3)}$$

In order for (E3.2) to be a correct assumption, it must satisfy both (E3.1) and (E3.3). First, satisfy (E3.3) as follows:

$$\frac{d^2v}{dx^2} = \frac{d}{dx^2}(a_0 + a_1x + a_2x^2 + a_3x^3 + a_4x^4) = 2a_2 + 6a_3x + 12a_4x^2 \quad \text{(E3.4)}$$

Satisfying (E3.3) with (E3.4) results in the following:

$$a_2 = 0, a_4 = -\frac{a_3}{2l} \quad \text{(E3.5)}$$

Substituting (E3.5) into (E3.2) gives the following:

$$v(x) = a_0 + a_1x + a_3x^3 - \frac{a_3}{2l}x^4 \quad \text{(E3.6)}$$

Satisfying (E3.3) gives the following for (E3.6)

$$a_0 = 0, a_1 = -\frac{a_3l^2}{2} \quad \text{(E3.7)}$$

Substituting (E3.7) into (E3.6) gives:

$$v(x) = a_3\left(-\frac{l^2x}{2} + x^3 - \frac{x^4}{2l}\right) \quad \text{(E3.8)}$$

Substituting (E3.8) into (E3.2) results in the following:

$$EI_{zz}\frac{d^4}{dx^4}\left[a_3\left(-\frac{l^2x}{2}+x^3-\frac{x^4}{2l}\right)\right]+P^T\frac{d^2}{dx^2}\left[a_3\left(-\frac{l^2x}{2}+x^3-\frac{x^4}{2l}\right)\right]=p_y \Rightarrow$$

$$p_y=-\frac{12a_3EI_{zz}}{l}+P^Ta_3\left(6x-6\frac{x^2}{l}\right) \qquad \text{(E3.9)}$$

Thus, the distributed loading given by (E3.9) provides the exact solution given by (E3.8).

b) The finite element solution for twelve elements of equal length is compared to the exact solution in Fig. 18, wherein it can be seen that convergence is obtained for a value of $a_3 = -0.001$.

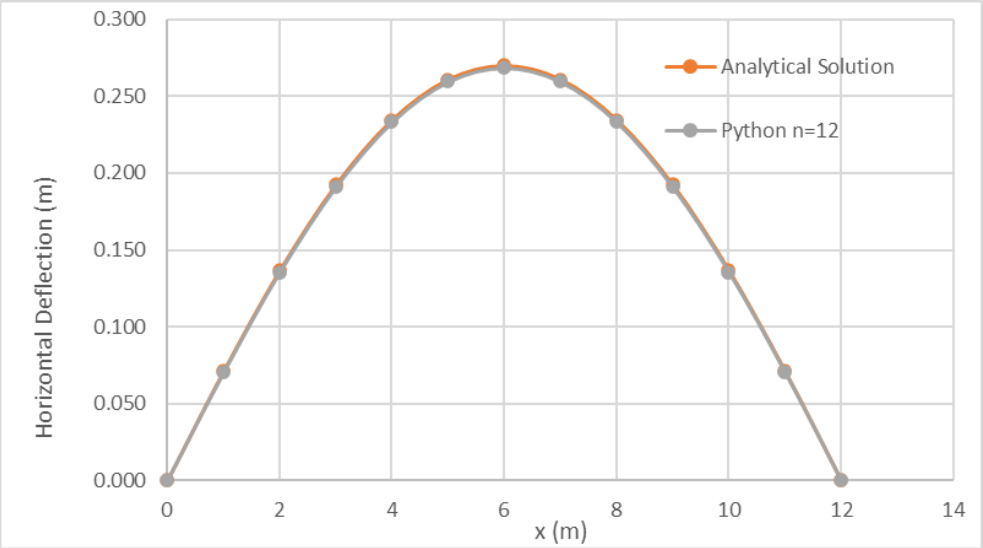

Figure 18 Comparison of Computational Result to Analytical Solution for Example Problem #3 in the Horizontal Plane

Example Problem #4

Given: A double-cantilevered beam is subjected to a distributed transverse load, where E=2.06x10^{11} N/m^2, I_{zz}=8.99x10^{-6} m^4, $k_y = k_y^0 = 10^5\ N/m^2$, A=0.0145 m^2 and l=12.0 m. In addition, $\alpha = 1.05x10^{-5}\ /°C$, $\Delta T = 50\ °C$ and $p_x = k_x = S = 0$.

Required: a) Find a form of $p_y = p_y(x)$ that provides an analytic solution for $v = v(x, p_y^0, E, I_{zz})$, assuming that $u(x) = 0, 0 \le x \le l$.

b) obtain a solution using finite elements and compare the two

Solution: a) The solution solves the following differential equation:

$$EI_{zz}\frac{d^4v}{dx^4} + P^T\frac{d^2v}{dx^2} + k_y v = p_y \qquad \text{(E4.1)}$$

Suppose that we choose the following:

$$v(x) = C_1\left[x^2 - \frac{2x^3}{l} + \frac{x^4}{l^2}\right] \quad 0 \le x \le l \qquad \text{(E4.2)}$$

where l is the length of the beam and C_1 is a loading constant. It can be seen that the above assumed solution satisfies the following boundary conditions:

$$v(x = 0, l) = 0$$
$$\frac{dv}{dx}(x = 0, l) = 0 \qquad \text{(E4.3)}$$

In order to obtain the forcing function, p_y, equation (E4.2) is now substituted into equation (E4.1) and solved, thereby resulting in the following:

$$p_y(x) = C_1 EI_{zz} \frac{d^4}{dx^4}\left[x^2 - \frac{2x^3}{l} + \frac{x^4}{l^2}\right] + C_1 P^T \frac{d^2}{dx^2}\left[x^2 - \frac{2x^3}{l} + \frac{x^4}{l^2}\right] + C_1 k_y^0 \left[x^2 - \frac{2x^3}{l} + \frac{x^4}{l^2}\right]$$

$$= \frac{24 C_1 EI_{zz}}{l^2} + C_1 P^T \left(2 - \frac{12x}{l} + \frac{12x^2}{l^2}\right) + C_1 k_y^0 \left[x^2 - \frac{2x^3}{l} + \frac{x^4}{l^2}\right] \quad \text{(E4.4)}$$

Equation (E4.2) is then the solution for a double cantilever beam with constant coefficient of friction and constant temperature change given by equation (2) subjected to forcing function given by equation (E4.4) and with boundary conditions (E4.3).

b) The finite element solution gives the results shown in Fig. 19 for the case wherein C_1=0.01.

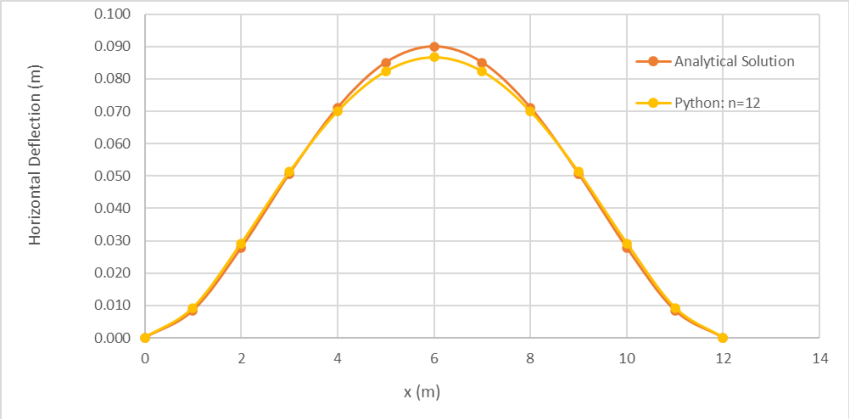

Figure 19 Comparison of Computational Result to Exact Solution for Example Problem #4 in the Horizontal Plane

It can be seen from the above example problem that the finite element model reproduces the exact solution for the linear case, with convergence obtained with 12 elements of equal length.

Modeling the Rail Response for the Nonlinear Case

Now consider the fifth term in equation (25) once again. The fifth term is nonzero and therefore nonlinear whenever there is axial displacement. Finally, consider the eighth and ninth terms in equation (25). These terms will necessarily be nonlinear whenever the coefficients of friction, k_x and k_y, are not constant, and this circumstance is the main purpose of the current study. The nonlinearity enters via the dependence of the friction coefficients on the displacement components, *u* and *v*, respectively. As shown in Fig. 20, single tie push tests (STPT) confirm the nonlinearity for the lateral coefficient k_y.

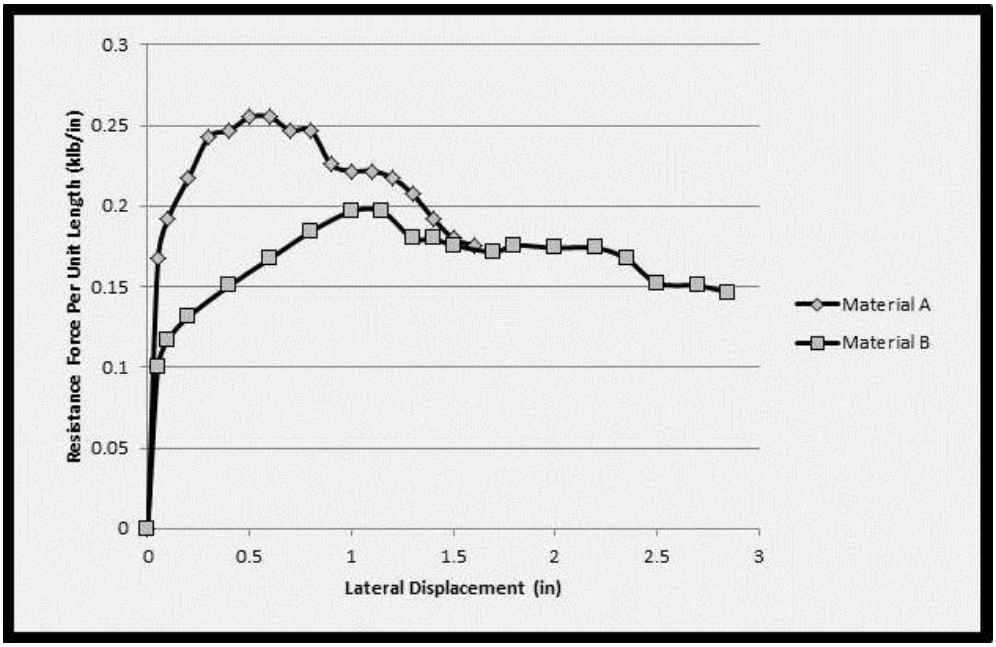

Figure 20 Typical Lateral Load vs. Displacement from STPT Tests (Read et al. 2011)

For a given rail structure configuration, the above response may be adequately modeled with a power law of the following form (Tvergaard and Needleman 1981, Allen et al. 2016):

$$k_y(v) = k_y^0 - k_y^1 \left(\frac{v}{v_0}\right)^n \tag{45}$$

It should be noted piecewise linear (Lim et al 2003), hyperbolic tangent equations (Grissom and Kerr 2006) and even upper limiting values (Grissom and Kerr 2006) have been used to curve fit the response illustrated in Fig. 20. However, the predicted buckling results do not appear to be very sensitive to the form of equations used. Thus, the power law form given by equation (45) is employed in this research. As shown in Fig. 21, this

type of curve fit does an adequate job of predicting the observed nonlinearity in the coefficient of lateral friction. Accordingly, the same type of equation is employed for the longitudinal coefficient of friction.

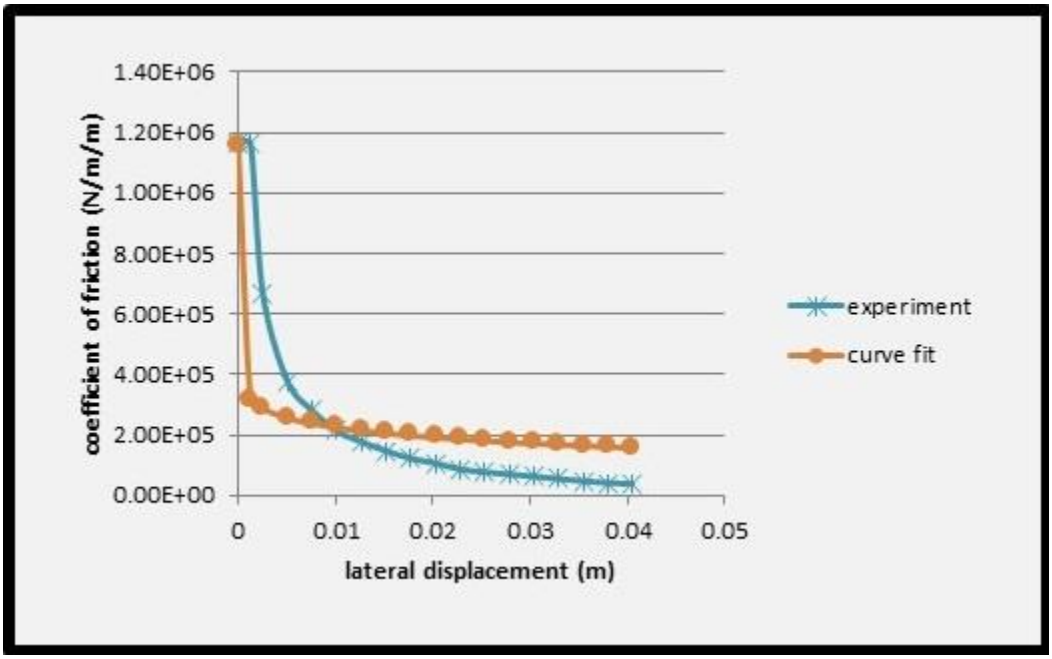

Figure 21 Comparison of Predicted Coefficient of Lateral Friction to Experimental Data Using Equation 45 (Reprinted with Permission from Allen and Fry, 2017)

As can be seen from Fig. 21, the coefficient of lateral friction can be highly nonlinear. Accordingly, failing to account for this nonlinearity in the model can lead to significant predictive error. Therefore, it is essential to include the ability to predict this nonlinearity in the model (Tvergaard and Needleman 1981, Lim et al. 2003, Grissom and Kerr 2006, Allen et al 2006). Toward this end, a standard time marching scheme is adopted herein, in which the externally applied mechanical load is gradually increased in

a series of time steps, with Newton iteration deployed to capture the nonlinearity on each time step (Little et al. 2016).

Briefly, this is accomplished by first obtaining an approximate solution in which it is assumed that in the term k_y the displacement from the previous time step is used, thereby resulting in the following initial approximation for the global form of equation (29).

$$\sum_{j=1}^{10} K_{ij}\,\Delta q_j^0 + \sum_{j=1}^{10} B_{ij}\,\Delta q_j^0 + \sum_{j=1}^{10} G_{ij}\,\Delta q_j^0 + \sum_{j=1}^{10} N_{ij}\,\Delta q_j^0 = \Delta F_i \qquad (46)$$

This erroneous value of $\Delta u^m(x)$ and $\Delta v^m(x)$ can be utilized to reduce the error by employing the following simple iteration method:

$$\begin{aligned} \left(G_{ij}\right)^{\eta} &= \left(G_{ij}(q_j^{\eta-1})\right) \\ \left(N_{ij}\right)^{\eta} &= \left(N_{ij}(q_j^{\eta-1})\right) \end{aligned} \qquad (47)$$

where η is the iteration number (Ketter and Prawel 1969, Little et al. 2016). Equation (46) is then reevaluated using the updated estimate of the matrices G_{ij} and N_{ij} obtained from equation (47). The iterative process is terminated when the following condition is satisfied:

$$\frac{\left\|\Delta q_i^{\eta} - \Delta q_i^{\eta-1}\right\|}{\left\|\Delta q_i^{\eta}\right\|} \leq e_{AL} \qquad (48)$$

where the double vertical lines signify the Euclidean norm, and e_{AL} is a preset value of allowable error. The total displacement field is subsequently evaluated as follows:

$$q_i(x(t+\Delta t)) = q_i(x(t)) + \Delta q_i^{\eta}(x(t+\Delta t)) \tag{49}$$

The above procedure is to be verified via example problems.

Validation Problems for the Nonlinear Case

The finite element algorithm is now validated for the nonlinear case with the following example problems.

Example Problem #5

Given: A beam that is simply supported at both ends is subjected to an incremental lateral distributed loading $p_y = const = 10\ N/m$, where E=2.06x10^{11} N/m^2, I_{yy}=I_{zz}=8.99x10^{-6} m^4, A=0.0145 m^2, l=12.0 m, and $p_x = p_z = k_x = k_y = k_z = S = \Delta T = 0$. The beam is subjected to an axial load, P, at the end x=0.

Required: a) Obtain an approximate analytic solution for $v = v(x)$ and determine the axial load, P_{cr}, that will cause the column to buckle.

b) Determine the location of the maximum lateral displacement and evaluate it.

c) Obtain a solution using the finite element method and compare the two.

Solution: a) The analytic solution solves the following variational equation:

$$\int_0^l EI_{zz}\frac{d^2v}{dx^2}\delta\left(\frac{d^2v}{dx^2}\right)dx + \int_0^l P\frac{dv}{dx}\delta\left(\frac{dv}{dx}\right)dx - \int_0^l p_y\delta v dx = 0 \tag{E5.1}$$

The analytic solution is assumed to be of the following form:

$$v(x) = a_1 + a_2 x + a_3 x^2 \tag{E5.2}$$

It follows that

$$\frac{dv}{dx}(x) = a_2 + 2a_3 x \tag{E5.3}$$

where the coefficients are to be determined. The displacement boundary condition on the left end implies that:

$$v(x = 0) = 0 \Rightarrow a_1 = 0 \tag{E5.4}$$

Thus, equation (E5.2) simplifies to the following:

$$v(x) = a_2 x + a_3 x^2 \tag{E5.5}$$

The displacement boundary condition on the right end implies that

$$v(x = l) = 0 = a_2 l + a_3 l^2 \Rightarrow a_2 = -a_3 l \tag{E5.6}$$

Substituting (5.6) into (5.5) therefore results in:

$$v(x) = C(x^2 - xl) \tag{E5.7}$$

where the coefficient *C* is to be determined by satisfying (E5.1). Substituting (E5.7) into (E5.1) thus results in the following:

$$\left(4EI_{zz}lC + \frac{1}{3}Pl^3C + \frac{1}{6}l^3p_y\right)\delta C = 0 \tag{E5.8}$$

Since δC is arbitrary, it follows that

$$C = -\frac{p_y l^2}{6}\left[\frac{1}{\left(\frac{1}{3}Pl^2 + 4EI_{zz}\right)}\right] \tag{E5.9}$$

Substituting (E5.9) into (E5.7) gives the displacement field:

$$v(x) = -\frac{p_y l^2}{6}\left[\frac{1}{\left(\frac{1}{3}Pl^2 + 4EI_{zz}\right)}\right](x^2 - xl) \tag{E5.10}$$

To obtain the buckling load, the second variation of equation (E5.8) is taken, thereby resulting in the following:

$$\left(4EI_{zz}l + \frac{1}{3}P_{cr}l^3\right)\delta C = 0 \tag{E5.11}$$

Since δC is arbitrary, it follows that

$$P_{cr} = -12\frac{EI_{zz}}{l^2} \tag{E5.12}$$

b) The maximum lateral displacement can be seen to occur at the midpoint of the beam, so that:

$$v_{\max} = v(x = l/2) = \frac{p_y l^4}{24}\left[\frac{1}{\left(4EI_{zz} + \frac{1}{3}Pl^2\right)}\right] \tag{E5.13}$$

Note also that the end rotation can also be evaluated by differentiating equations (E5.13) as follows:

$$\theta(x) \equiv \frac{dv}{dx}(x) = -\frac{p_y l^2}{6}\left[\frac{1}{\left(\frac{1}{3}Pl^2 + 4EI_{zz}\right)}\right](2x - l) \tag{E5.14}$$

The predicted value of $\theta(x=0) = \theta_0$ can now be substituted into the above to obtain the following:

$$\theta_0 = \frac{p_y l^3}{6}\left[\frac{1}{\left(4EI_{zz} + \frac{1}{3}Pl^2\right)}\right] \tag{E5.15}$$

Substituting the above result back into equation (E5.13) thus gives the following:

$$v_{\max}^{FE} = \theta_0 l / 4 \qquad \text{(E5.16)}$$

c) In order to account for the coupling between the axial and lateral displacement components it is necessary to solve the problem with multiple elements using the finite element method. Fig. 22 shows the results of the finite element prediction using six elements of equal length, wherein it can be seen that both the predicted maximum displacement buckling load match the results obtained above.

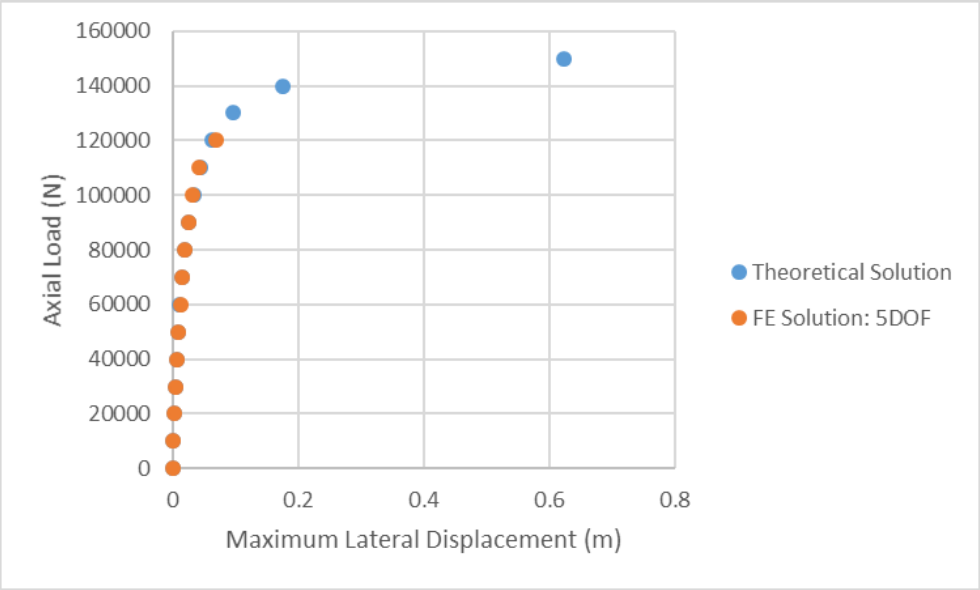

Figure 22 Comparison of Finite Element Approximation to Variational Solution for Example Problem #5

Example Problem #6

Given: A double-cantilevered beam is subjected to a distributed loading, where E=2.06x10^{11} N/m^2, I_{yy}=I_{zz}=8.99x10^{-6} m^4, A=0.0145 m^2, l=12.0 m,$\alpha = 1.05x10^{-5}\ /°C$, $p_x = p_z = k_x = k_z = S = 0$ and $\Delta T = 50\ °C$. In addition, the lateral coefficient of friction parameters used to fit the data in Fig. 22 are $k_y^0 = 1.16x10^6 N/m^2$, $k_y^1 = 6.5x10^5 N/m^2$, $v_0 = 0.005\ m$ and n=0.05.

Required: a) Obtain an analytic solution for $v = v(x, p_y^0, E, I_{zz})$.

b) Obtain a solution using finite elements and compare the two

Solution: a) The solution solves the following differential equation:

$$EI_{zz}\frac{d^4v}{dx^4} + P^T\frac{d^2v}{dx^2} + k_y v = p_y \tag{E6.1}$$

Suppose that we choose the following:

$$v(x) = C_1\left[x^2 - \frac{2x^3}{l} + \frac{x^4}{l^2}\right] \quad 0 \le x \le l \tag{E6.2}$$

where l is the length of the beam and C_1 is a loading constant. It can be seen that the above assumed solution satisfies the following boundary conditions:

$$v(x = 0, l) = 0$$
$$\frac{dv}{dx}(x = 0, l) = 0 \tag{E6.3}$$

In order to obtain the forcing function, p_y, equation (E6.2) is now substituted into equation (E6.1) and it is solved, thereby resulting in the following:

$$p_y(x) = C_1 EI_{zz} \frac{d^4}{dx^4}\left[x^2 - \frac{2x^3}{l} + \frac{x^4}{l^2}\right] + C_1 P^T \frac{d^2}{dx^2}\left[x^2 - \frac{2x^3}{l} + \frac{x^4}{l^2}\right] +$$

$$+C_1\left[k_y^0 - k_y^1\left[\frac{C_1\left[x^2 - \frac{2x^3}{l} + \frac{x^4}{l^2}\right]}{v_0}\right]^n\right]\left[x^2 - \frac{2x^3}{l} + \frac{x^4}{l^2}\right] = \frac{24C_1 EI_{zz}}{l^2} +$$

$$+C_1 P^T\left(2 - \frac{12x}{l} + \frac{12x^2}{l^2}\right) + C_1\left[k_y^0 - k_y^1\left[\frac{C_1\left[x^2 - \frac{2x^3}{l} + \frac{x^4}{l^2}\right]}{v_0}\right]^n\right]\left[x^2 - \frac{2x^3}{l} + \frac{x^4}{l^2}\right] \quad \text{(E6.4)}$$

The above forcing function will produce the displacement field given in equation (E6.2).

b) The next step is to compare the computational results obtained with the finite element algorithm to the exact solution represented by equations (E6.2) and (E6.4). Toward this end, an allowable error of $e_{AL} = 5.0X10^{-6}$ has been utilized. Fig. 23 shows the predicted vs. exact results for three different element meshes. On the basis of these results it is concluded that a 20-element mesh is sufficiently accurate for the purpose of approximating the displacement field within a rail structure modeled by equations (11)-(19). Furthermore, Fig. 24 shows the finite element predictions using the 20-element mesh on a few different iterations. On the basis of this, it is concluded that only a few iterations are necessary to accurately predict the effects of nonlinearity in the friction between the ballast-crosstie interface.

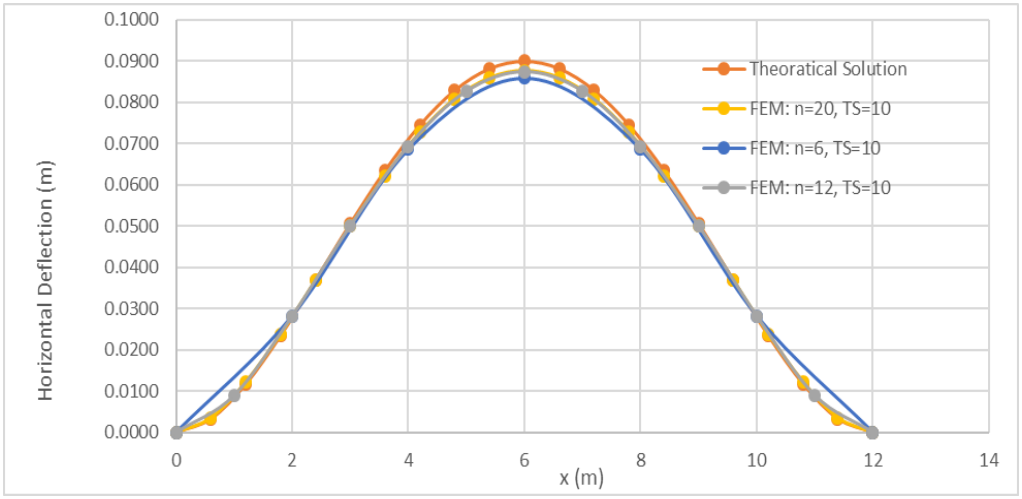

Figure 23 Comparison of Finite Element Approximations for Three Different Meshes to Theoretical Solution for Example Problem #6

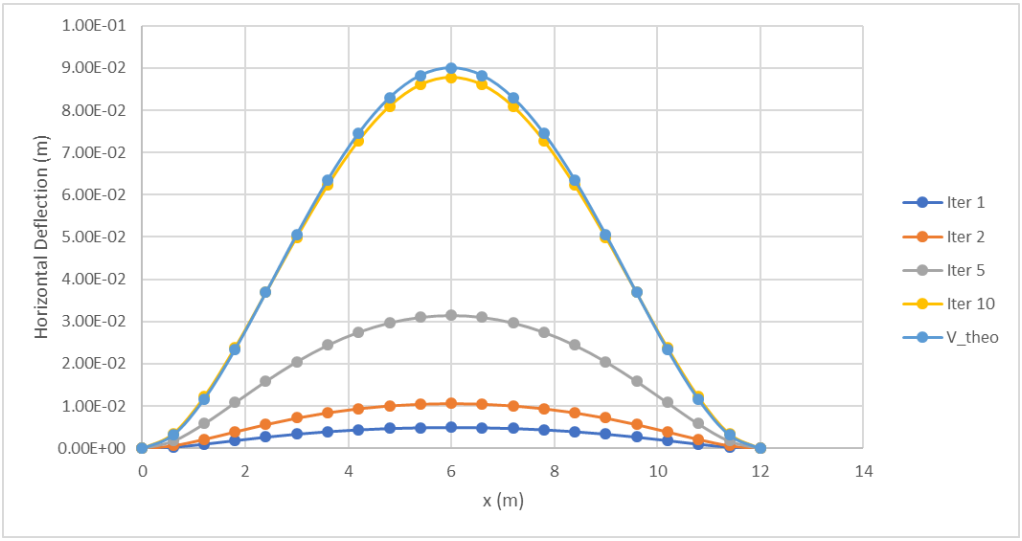

Figure 24 Comparison of Finite Element Approximations for Different Iterations (20 element mesh) to Theoretical Solution for Example Problem #6

Example Problem #7

Given: A beam that is cantilevered at one end and simply supported at the other is subjected to a constant lateral distributed loading $p_y = const = 10\ N/m$, where E=2.06x10^{11} N/m^2, I_{zz}=8.99x10^{-6} m^4, A=0.0145 m^2, l=12.0 m, and $p_x = k_x = k_y = S = \Delta T = 0$. The beam is subjected to an axial load, P, at the simply supported end.

Required: a) Obtain an approximate analytic solution for $v = v(x)$ and determine the axial load, P_{cr}, that will cause the column to buckle.

b) Determine the location of the maximum lateral displacement and evaluate it.

c) Obtain a solution using the finite element method and compare the two.

Solution: a) The analytic solution solves the following variational equation:

$$\int_0^l EI_{zz} \frac{d^2v}{dx^2} \delta\left(\frac{d^2v}{dx^2}\right) dx - \int_0^l P \frac{dv}{dx} \delta\left(\frac{dv}{dx}\right) dx - \int_0^l p_y \delta v dx = 0 \qquad \text{(E7.1)}$$

The analytic solution is assumed to be of the following form:

$$v(x) = a_1 + a_2 x + a_3 x^2 + a_4 x^3 + a_5 x^4 \qquad \text{(E7.2)}$$

It follows that

$$\frac{dv}{dx}(x) = a_2 + 2a_3x + 3a_4x^2 + 4a_5x^3 \tag{E7.3}$$

where the coefficients are to be determined. The boundary conditions on the left end are as follows:

$$v(x=0) = 0 \Rightarrow a_1 = 0 \tag{E7.3a}$$

$$\frac{M_z}{EI_{zz}}(x=0) = 0 \Rightarrow a_3 = 0 \tag{E7.3b}$$

Thus, equation (E7.2) simplifies to the following:

$$v(x) = a_2x + a_4x^3 + a_5x^4 \tag{E7.4}$$

The boundary conditions on the right end are as follows:

$$v(x=l) = 0 \Rightarrow a_2 = -a_4l^2 - a_5l^3 \tag{E7.5a}$$

$$\frac{dv}{dx}(x=l) = 0 \Rightarrow a_2 = -3a_4l^2 - 5a_5l^3 \tag{E7.5b}$$

Reducing the above two equations to a single unknown C gives the following:

$$v(x) = C\left(l^3 x - 3lx^3 + 2x^4\right) \tag{E7.6}$$

where the coefficient C is to be determined by satisfying (E7.1). Substituting (E7.6) into (E7.1) thus results in the following:

$$\left(\frac{36}{5} EI_{zz} l^5 C - \frac{72}{210} Pl^7 C - \frac{3}{20} l^5 p_y\right)\delta C = 0 \tag{E7.7}$$

Since δC is arbitrary, it follows that

$$C = \frac{3p_y}{20}\left[\frac{1}{\left(\frac{36}{5} EI_{zz} - \frac{72}{210} Pl^2\right)}\right] \tag{E7.8}$$

Substituting (E7.8) into (E7.6) gives the displacement field:

$$v(x) = \frac{3p_y}{20}\left[\frac{1}{\left(\frac{36}{5} EI_{zz} - \frac{72}{210} Pl^2\right)}\right]\left(l^3 x - 3lx^3 + 2x^4\right) \tag{E7.9}$$

To obtain the buckling load, the second variation of equation (E7.7) is taken, thereby resulting in the following:

$$\left(\frac{36}{5}EI_{zz} - \frac{72}{210}P_{cr}l^2\right)\delta C = 0 \qquad \text{(E7.10)}$$

Since δC is arbitrary, it follows that

$$P_{cr} = 21\frac{EI_{zz}}{l^2} \qquad \text{(E7.11)}$$

b) The maximum lateral displacement can be obtained by taking the derivative of equation (E7.7) and setting it to zero. This will result in the following:

$$v_{\max} \cong v(x = 0.4l) \cong 0.039\,p_y l^4 \left[\frac{1}{\left(\frac{36}{5}EI_{zz} - \frac{72}{210}Pl^2\right)}\right] \qquad \text{(E7.10)}$$

c) Since the analytic solution is cubic in *x*, the finite element solution can be obtained by using a single finite element. The buckling load is determined by incrementally increasing the axial load until an instability occurs in the predicted results. Fig. 25 shows the results of the finite element prediction, wherein it can be seen that both the

predicted maximum displacement matches equation (E7.10) and the predicted buckling load matches equation (E7.9).

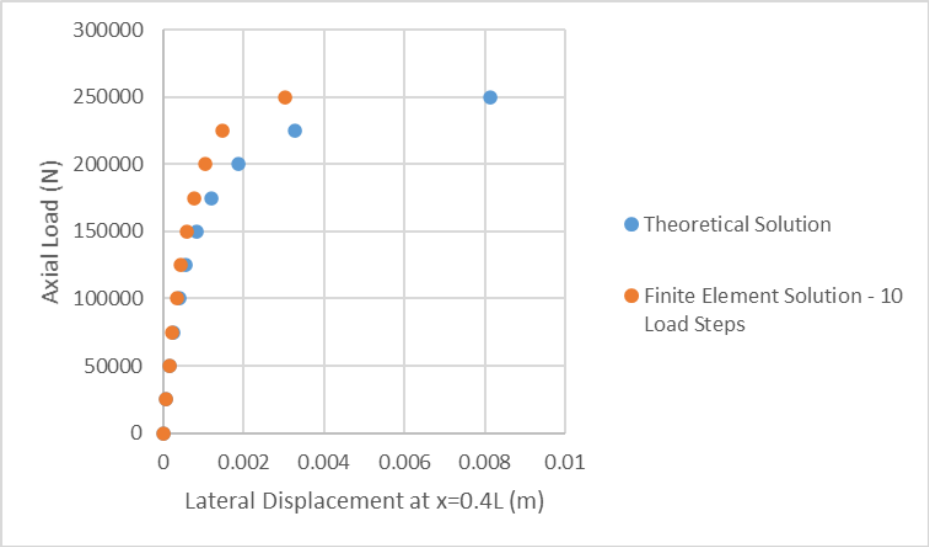

Figure 25 Comparison of Finite Element Approximation (10 elements mesh) to Analytical Solution for Example Problem #7

Validation Problems for the Case of Lift-Off

In general, lift-off induced buckling occurs due to the geometry of the rail structure and the loss in friction the ballast typically would exert on the track during downward vertical motion. Firstly, due to the geometry of the rail cross-section, buckling normally occurs about the horizontal x-y plane because I_{yy} is much greater than I_{zz}, meaning that the rail will fail about the weak z-z axis. Furthermore, even when the rail bends about the y axis, buckling will occur about the z axis. Additionally, when the rail lifts off, the friction goes to zero, thus removing the resistance to motion exerted on the rail from the ballast, thereby inducing buckling. Figure 26, shown below, depicts this phenomenon.

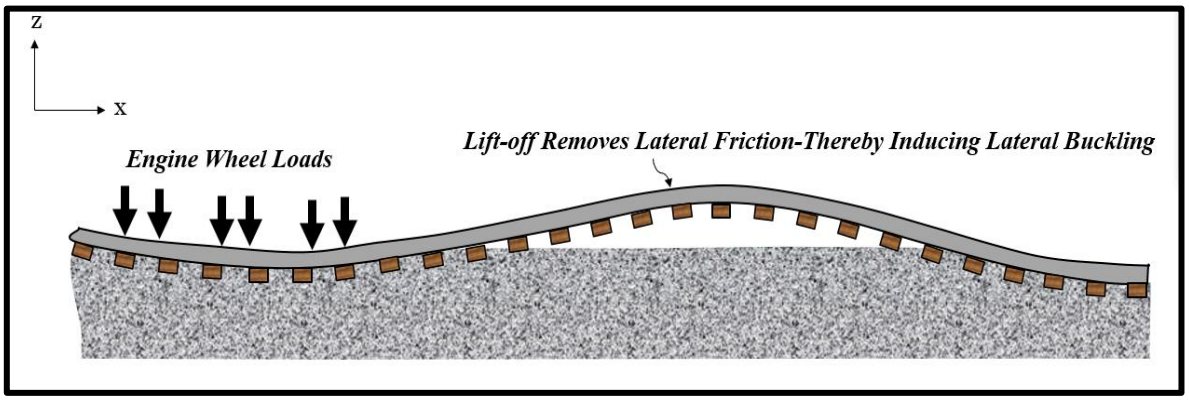

Figure 26 Depiction of the Rail Lift-off Problem

The finite element algorithm is now validated for the lift-off case with the following example problem.

Example Problem #8

Given: A beam that is resting on an elastic foundation is subjected to a concentrated vertical load, as shown in Fig. 27, with $F_z = const = 1000\ N$. In addition, E=2.06x10^{11} N/m^2, $I_{yy}=I_{zz}$=8.99x10^{-6} m^4, A=0.0145 m^2, l=12.0 m, $k_z = 1.16x10^6\ N/m^2$ and $p_x = p_y = p_z = k_x = k_y = S = \Delta T = 0$.

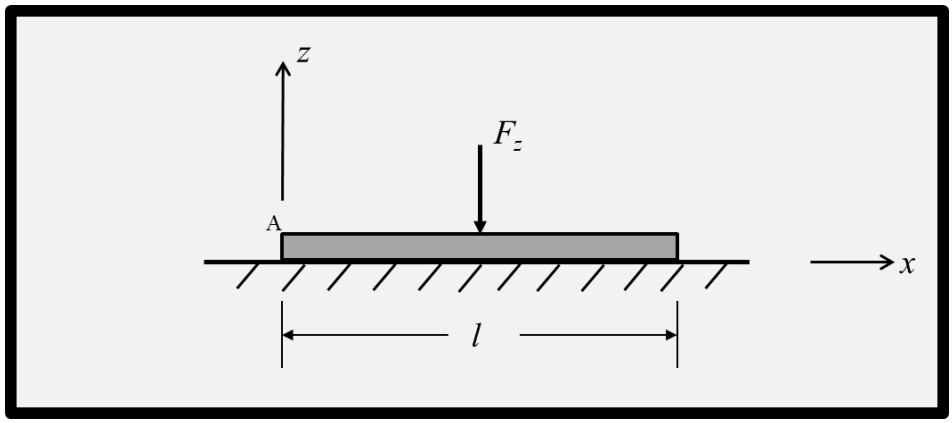

Figure 27 Depiction of a Prismatic Beam Resting on an Elastic Foundation Subjected to Concentrated Loading

Required: a) Obtain an analytic solution for $w = w(x)$.

b) Obtain a solution using the finite element method and compare the two.

Solution: a) The analytic solution solves the following differential equation:

$$\frac{d^2}{dx^2}\left(EI_{zz}\frac{d^2w}{dx^2}\right) + k_z w = p_z \tag{E8.1}$$

In order to obtain an analytical solution for this structure, (E8.1) can be simplified and rewritten as:

$$\frac{d^4w}{dx^4} + 4\beta^4 w = 0 \tag{E8.2}$$

where:

$$\beta = \sqrt[4]{\frac{k_z}{4EI_{yy}}} \tag{E8.3}$$

The analytic solution to this equation is found to be (Oden and Ripperger 1981) as follows:

$$w(x) = \delta_A \cosh(\beta x)\cos(\beta x) + \frac{\theta_A}{2\beta}\left(\sinh(\beta x)\cos(\beta x) + \cosh(\beta x)\sin(\beta x)\right) \tag{E8.4}$$

where δ_A and θ_A represent the unknown deflection and slope at the end A of the beam, respectively. The unknown coefficient θ_A can be solved for by imposing symmetry of the slope as follows:

$$\frac{dw}{dx}\left(\frac{l}{2}\right) = 0 \tag{E8.5}$$

which results in the following:

$$\theta_A = -\delta_A \beta \left(\tanh\left(\frac{\beta l}{2}\right) - \tan\left(\frac{\beta l}{2}\right)\right) \tag{E8.6}$$

Substituting (E8.6) into (E8.4) and setting the sum of all the forces in the vertical direction equal to zero, results in the following:

$$\delta_A = \beta F_z \left\{ k_z \left[\sinh\left(\frac{\beta l}{2}\right) \cos\left(\frac{\beta l}{2}\right) + \cosh\left(\frac{\beta l}{2}\right) \sin\left(\frac{\beta l}{2}\right) - \left(\tanh\left(\frac{\beta l}{2}\right) - \tan\left(\frac{\beta l}{2}\right) \right) \left(\sinh\left(\frac{\beta l}{2}\right) \sin\left(\frac{\beta l}{2}\right) \right) \right] \right\}^{-1} \quad \text{(E8.7)}$$

Thus, (E8.4) and (E8.7) represent the analytical solution to (E8.1) on the left-hand side of the beam. Note that on the right-hand side of the beam, (E8.1) becomes:

$$w(x) = \delta_A \cosh(\beta(l-x))\cos(\beta(l-x)) + \frac{\theta_A}{2\beta}\left(\sinh(\beta(l-x))\cos(\beta(l-x)) + \cosh(\beta(l-x))\sin(\beta(l-x))\right) \quad \text{(E8.8)}$$

c) The finite element solution is obtained using 6 elements of equal length. Comparative results are shown in Fig. 28.

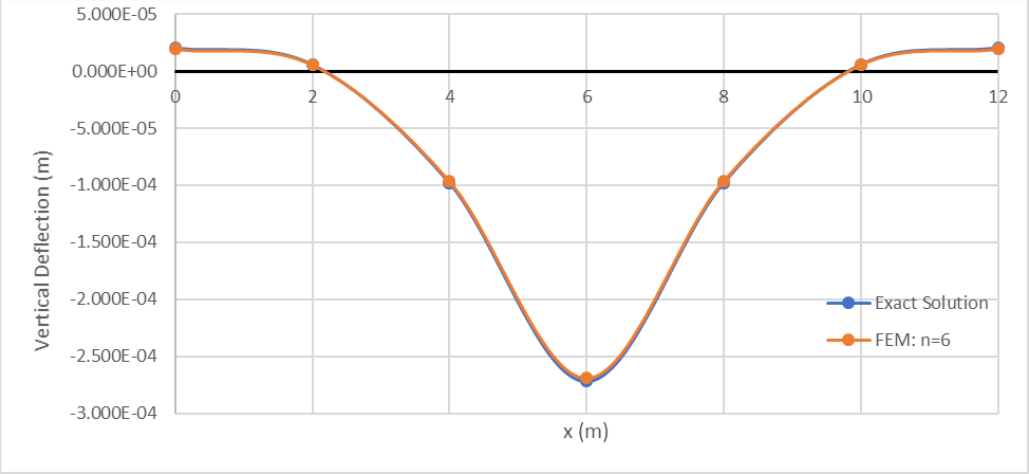

Figure 28 Comparison of Computational Result to Exact Solution for Example Problem #8

This completes the validation of the computational model for predicting buckling in rails.

CHAPTER VI

RESULTS

The following sections of this report illustrate the results of the research efforts to date. Briefly, these efforts are focused on mitigating rail buckling via sensitivity analysis. Most recently, the focus has been on modeling the effects of rail lift-off on lateral buckling.

Analysis of Sensitivity of Buckling due to Variations in Rail Physics

The rail buckling model developed herein is being deployed for the purpose of prioritizing rail buckling mitigation strategies. Toward this end, sensitivity studies were performed for the following variables: temperature change (ΔT), lateral friction coefficient (k_y), rotational stiffness (also known as rail pinning, S), lateral track walk and vertical coefficient of friction (known as track modulus, k_z).

The sensitivity is the rate of change of the buckling load with respect to the target variable. It can be seen that this is represented by the slope in the following diagrams, whereby the effects on the buckling load due to a change in the variable of interest can be assessed. Symmetric (u-shaped) buckles were therefore modelled on 40-foot-long sections of the rail, induced by monotonically increasing both the axial and transverse loading until buckling occurs in the rail structure.

Temperature Sensitivity

First consider the sensitivity of the buckling load to changes in temperature. As shown in Fig. 29, the predicted buckling load decreases with increasing temperature change. The sensitivity of the buckling load is the slope of the curve, whereby it can be

observed that there is a slight increase in sensitivity of the buckling load to temperature change with increasing temperature change.

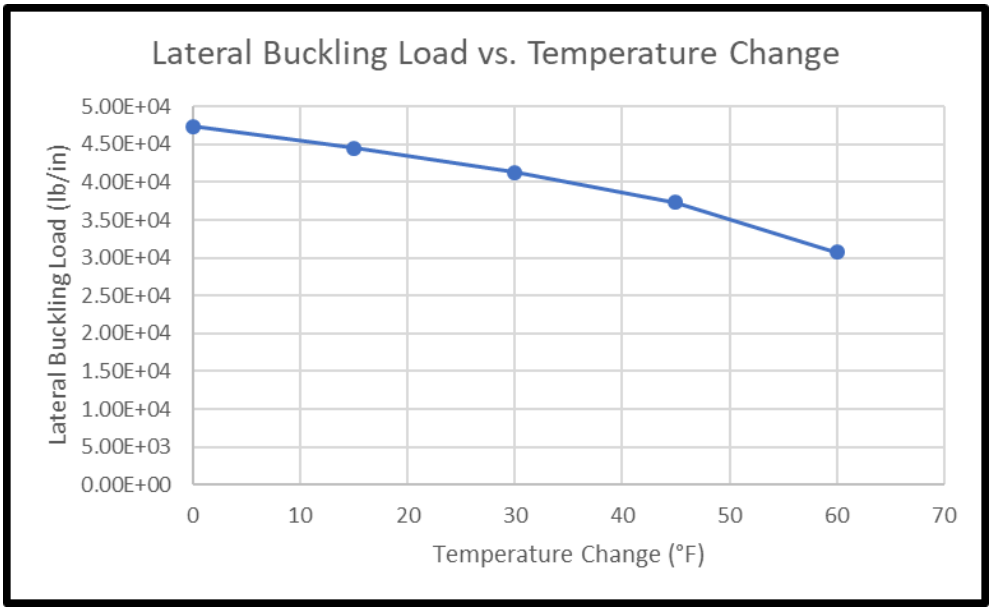

Figure 29 Predicted Effect of Temperature Change on Buckling Resistance of a Typical Rail Structure

Lateral Coefficient of Friction Sensitivity

Consider now the sensitivity of the buckling load to changes in the lateral coefficient of friction, which represents the transverse component of friction between the ballast and the crosstie. As shown in Fig. 30, the predicted buckling load increases with increasing coefficient of lateral friction. Furthermore, there is no observed change in the sensitivity with increasing ballast-crosstie friction.

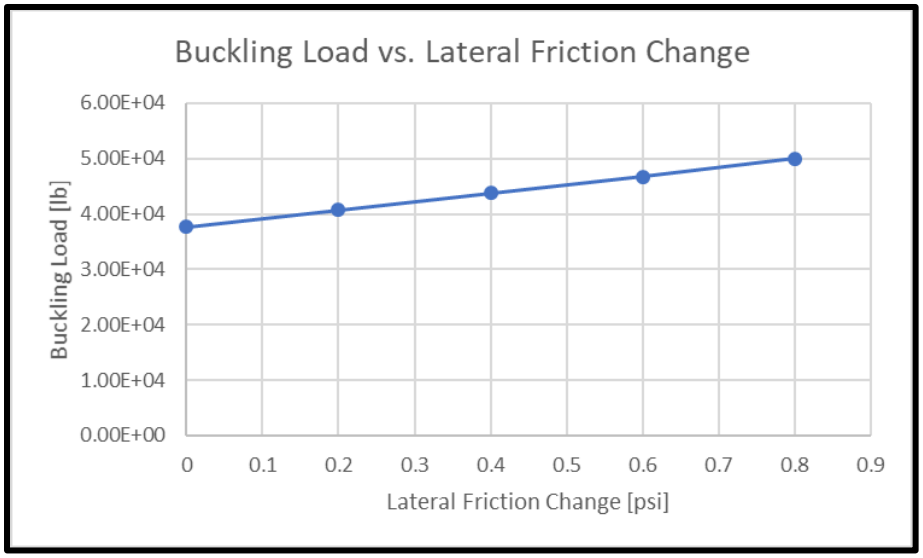

Figure 30 Predicted Effect of Ballast-Crosstie Coefficient of Lateral Friction Change on Buckling Resistance of a Typical Rail Structure

Rail Pinning Sensitivity

Consider next the sensitivity of the buckling load to changes in rotational stiffness (rail pinning), which, as previously explained, represents the crosstie-fastener resistance to the rotation of the track. As shown in Fig. 31, the predicted buckling load decreases with increasing rotational stiffness. Small or negligible change in the sensitivity can be observed with increasing resistance to track rotation.

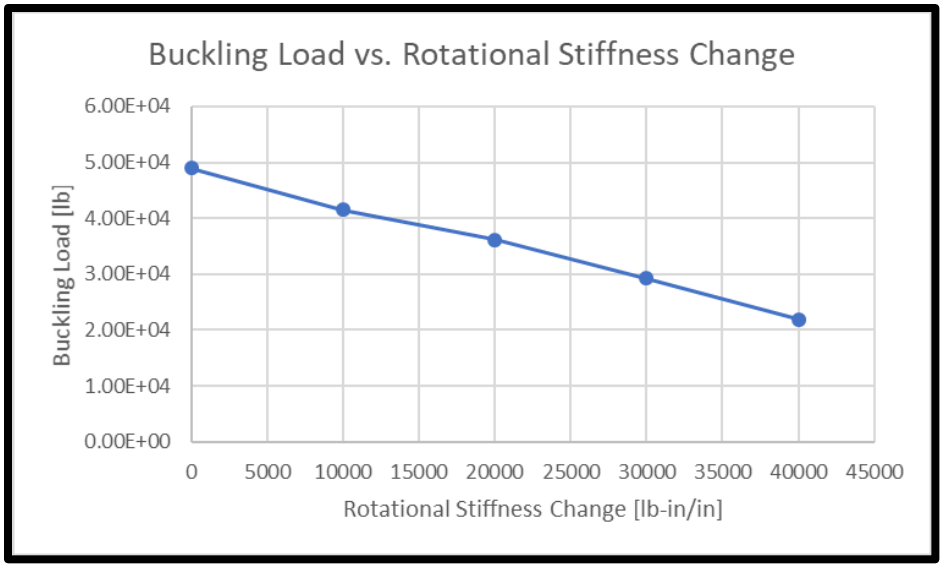

Figure 31 Predicted Effect of Rotational Stiffness Variation on Buckling Resistance of a Typical Rail Structure

Lateral Track Walk Sensitivity

Consider now the sensitivity of the buckling load to changes in initial lateral deformation, often referred to as lateral track walk. As shown in Fig. 32, the predicted buckling load decreases with increasing lateral track walk. The sensitivity appears to behave nonlinearly and changes in the magnitude of the lateral track walk of at least 0.5-in are observed to affect it significantly.

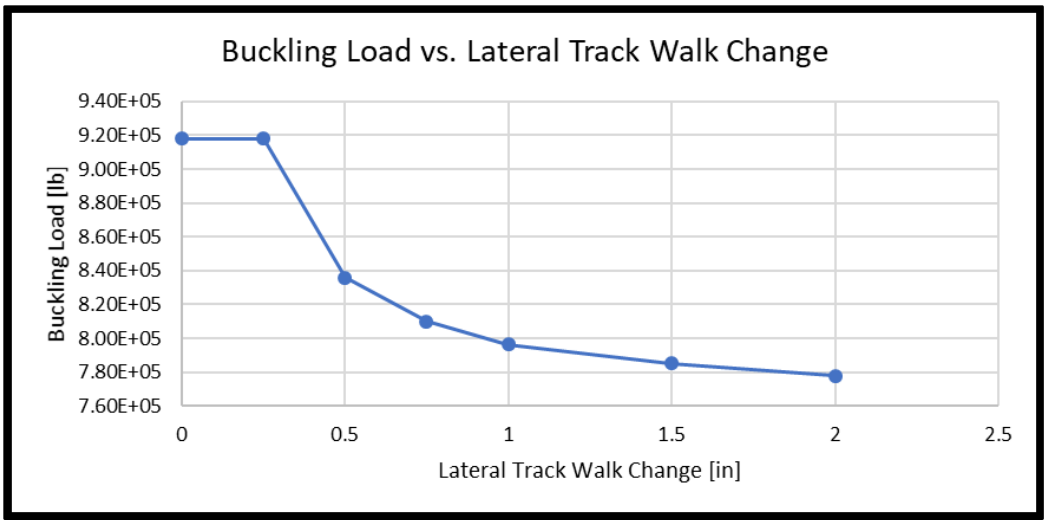

Figure 32 Predicted Effect of Lateral Track Walk Change on Buckling Resistance of a Typical Rail Structure

Vertical Lift-Off Sensitivity

Lastly, consider the sensitivity of the buckling load to changes in track modulus, k_z, which represents the vertical component of friction acting at the interface of the ballast with the rail structure. The track modulus is therefore defined as a measure of the vertical stiffness of the rail foundation (Selig and Li 1994), which represents the elastic modulus of the foundation. In order to fully investigate the sensitivity of the buckling load to changes in track modulus, it was necessary to consider both the cases of no lift-off and that of vertical lift-off of the track structure. The sensitivity to changes in the magnitude of the track modulus are therefore shown for both cases in Fig. 33 and 34, respectively. From Fig. 33, it can be clearly inferred that when the rail does not lift-off, the buckling load is insensitive to changes in k_z. However, as shown in Fig. 34, the buckling load is significantly affected by changes in track modulus when the track structure experiences lift-off. The sensitivity for this case is highly nonlinear, and it can be inferred that lift-off

resulting from a softer foundation removes resistance due to lateral friction thereby dramatically reducing the buckling load. Note that typical values of k_z (Kerr 2000) were utilized in these results (800-6000-lb/in^2).

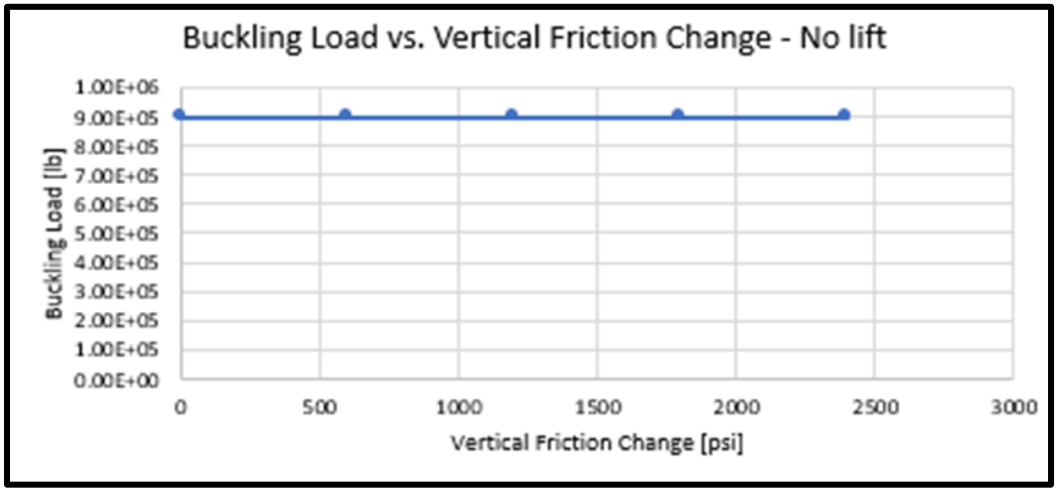

Figure 33 Predicted Effect of Track Modulus on Buckling Resistance of a Typical Rail Structure for the Case of No Lift-Off

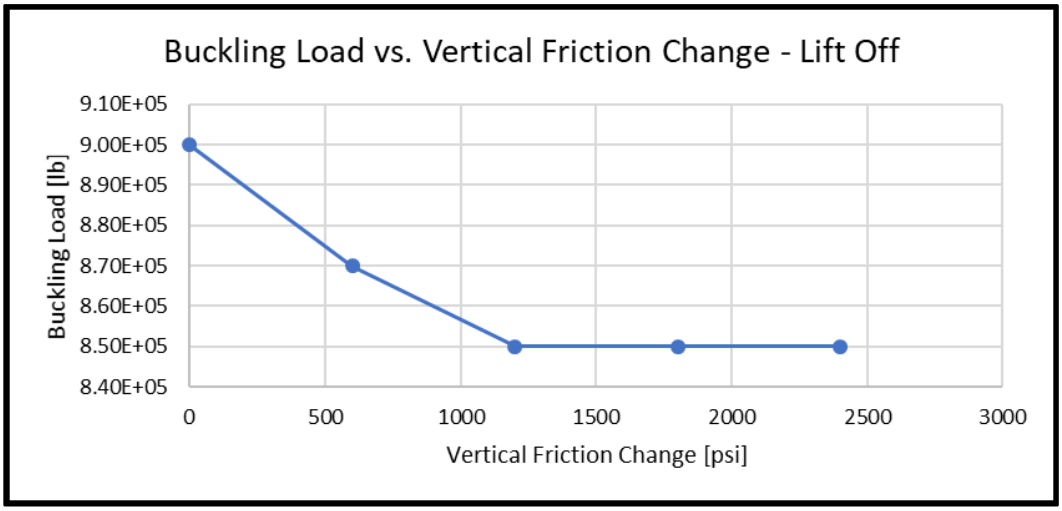

Figure 34 Predicted Effect of Track Modulus on Buckling Resistance of a Typical Rail Structure for the Case of Lift-Off

Summary of Lift-Off Induced Lateral Thermal Buckling

The model presented herein was deployed in an effort to analyze the effects of track lift-off on lateral buckling, with the objective of validating the following hypotheses:

I. Lift-off is inversely proportional to the track modulus (k_z)
II. The buckling load is a strong function of the track modulus (k_z) when lift-off occurs
III. When lift-off does not occur, the buckling load is a weak function of the track modulus (k_z)

Due to the geometric shape of the cross-section of the rail, $I_{yy} \gg I_{zz}$, so buckling vertically (about the y axis) rarely if ever happens in rails. Based on industry observations, what typically happens is that the rail lifts vertically and buckles laterally.

In order to accurately predict the response of the rail structure to vertical displacement, the same assumption implemented in at least one more complex model (Dong, Sankar and Dukkipati 1994) has been incorporated as follows:

$$\forall w(x) > 0 \quad \Rightarrow \quad k_x = k_y = k_z = 0 \tag{50}$$

Equation (50) ensures that whenever the track system lifts off from the ballast the coefficients of friction are taken as zero. This relationship is checked at every time step and iteration of the model.

The results presented above are consistent with the results of the sensitivity analysis previously presented, and will be validated by comparing the buckling load of a

very long section of track structure that is induced to buckle asymmetrically (s-shaped) for the cases of no-lift and lift-off induced buckling.

Example Problem #9

Case 1: No Lift-Off

Given: A beam that is cantilevered at one end and pinned at the other is subjected to a compressive axial load P = 50,000 lb, a transverse constant distributed load $p_y = const = 10\ lb/ft^2$, and a vertical constant distributed load $p_z = const = -10\ lb/ft^2$,. In addition, E=4.30x10^9 *lb/ft*^{2}, I_{yy} = 6.35x10^{-3} *ft*^{4}, *Izz*= 8.99x10^{-6} *ft*^{4}, A=1.56x10^{-1} *ft*^{2}, l=250 *ft*, $k_x = k_y = 28.8$ *lb/ft*^{2}, $\Delta T = 15\ °F, \alpha = 5.83x10^{-6}\ 1/°F$ *and* $p_x = k_z = S = 0$.

Case 2: Lift-Off

Given: A beam that is cantilevered at one end and pinned at the other is subjected to a compressive axial load P = 17,000 lb, a transverse constant distributed load $p_y = const = 10\ lb/ft^2$, and 6 vertical concentrated loads $F_z = -50{,}000\ lb$ located within 60 ft from the cantilevered end of the beam. In addition, E=4.30x10^9 *lb/ft*^{2}, I_{yy} = 6.35x10^{-3} *ft*^{4}, *Izz*= 8.99x10^{-6} *ft*^{4}, A=1.56x10^{-1} *ft*^{2}, l=250 *ft*, $k_x = k_y = 28.8$ *lb/ft*^{2}, $k_z = 80$ *lb/ft*^{2} , $\Delta T = 15\ °F, \alpha = 5.83x10^{-6}\ 1/°F$ *and* $p_x = S = 0$.

Required: a) Use the finite element method to obtain the magnitude of the buckling load for case 1 and case 2 and compare the two.

Solution: a) The finite element solution was obtained for a mesh of 25 elements and 200 iterations. The buckling load is determined by incrementally increasing the axial load until

an instability occurs in the predicted results. Fig. 35 shows the results of the finite element prediction for both case 1 and case 2.

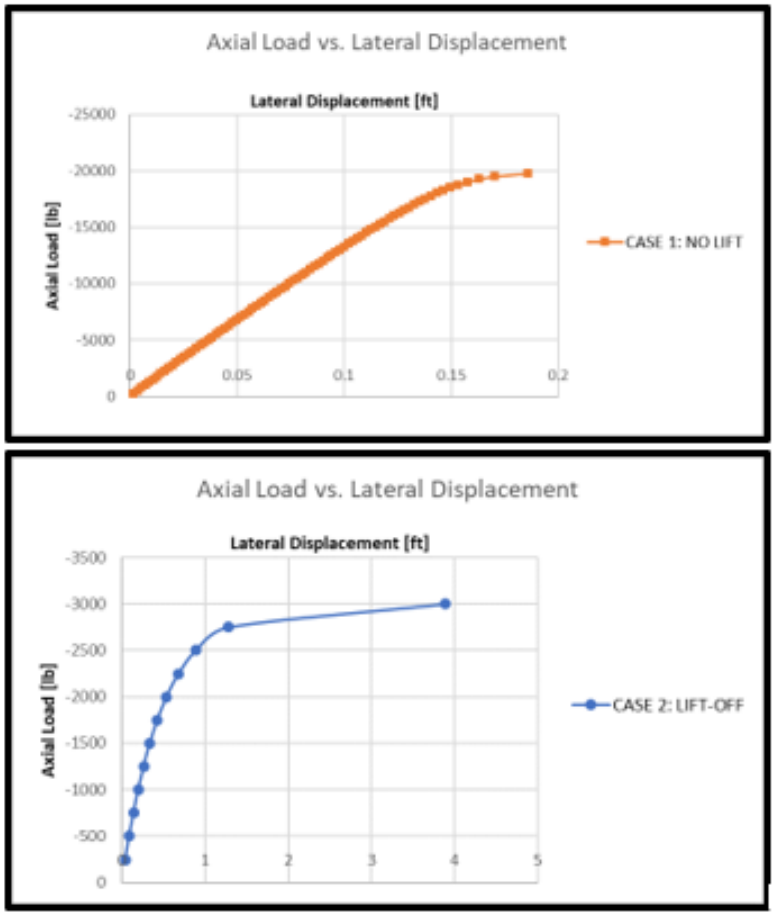

Figure 35 Comparison of Finite Element Approximations for Different Iterations of the Buckling Load Obtained for Case 1 (top) and Case 2 (bottom)

The buckling load for the case of no lift-off was found to be 20,000-lb (C). The lift-off case was then simulated with an axial load P = 17,000-lb (C). The buckling load for the lift-off case was then found to be 3,000-lb (C). It was therefore shown that the buckling load decreases significantly with lift-off of the track structure and is thus dependent on the track modulus. Note once again that lift-off is predicted only for

circumstances wherein the track modulus is relatively low. Finally, for extremely small values of k_z, lift-off is entirely mitigated so that buckling is once again obviated. Note that the lift-off problem was modeled up utilizing arbitrary values of the coefficients of friction, as further research outside the scope of this paper is expected to properly establish realistic friction coefficients for the rail structure. However, the track modulus was estimated to typically range between 800 and 6000 psi (Kerr 2000) for rail structures, and therefore this range was utilized to show vertical amplitude and axial extension as function of the track modulus as shown in Fig. 36.

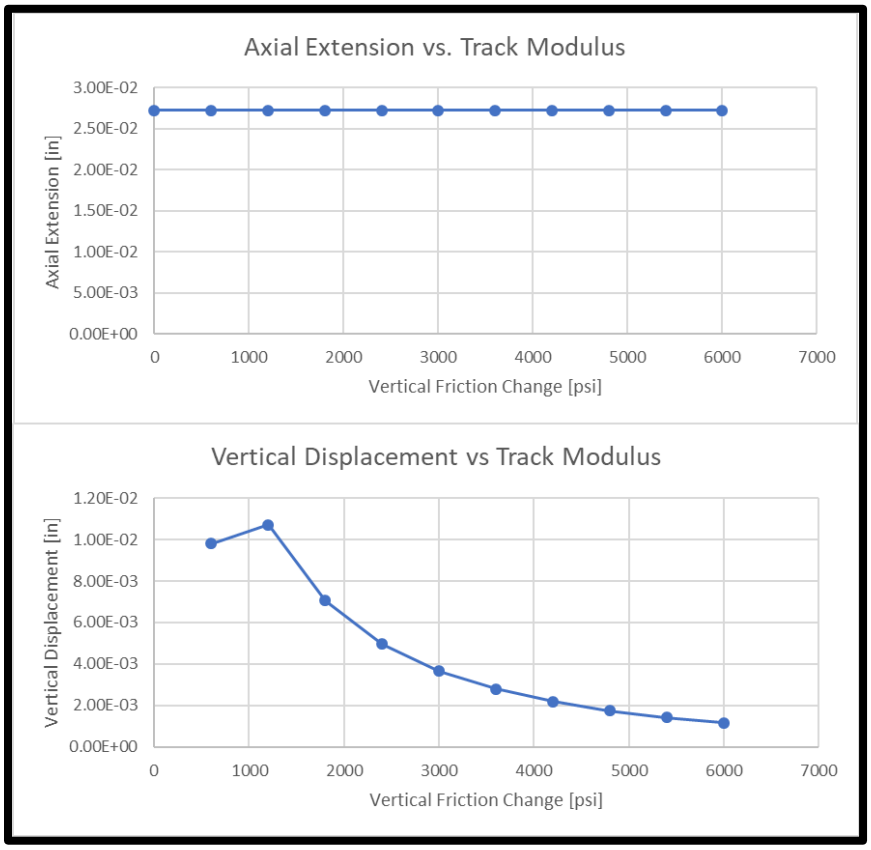

Figure 36 Axial Extension (top) and Vertical Amplitude (bottom) as Functions of the Track Modulus

Therefore, it can be seen that for the lift-off case, axial extension at the buckling load is not sensitive to variations of the track modulus, as expected due to the fact that axial deformation depends on axial loading and does not depend on k_z. However, vertical deformation at lift-off is highly dependent on the track modulus, and Fig. 36 further corroborates the hypothesis that lift-off is induced by relatively low track modulus and additionally, that there exists an even smaller value of the track modulus for which lift-off does not occur. Finally, Fig 36 shows that there also exists a range of really high values of the track modulus for which lift-off is also mitigated, thus also obviating lateral buckling.

CHAPTER VII

CONCLUSIONS*

A formulation has been presented herein for the purpose of modeling lateral buckling in rail structures resting on ballast with nonlinear coefficients of friction, and this formulation has been cast within a nonlinear finite element formulation. The formulation has been validated against both linear and nonlinear example problems where closed-form solutions exist, and it has been shown that the formulation presented herein is both efficient and accurate when compared to analytical solutions.

Unfortunately, analytical solutions do not exist for the vast majority or realistic circumstances involving rail structures, and this comprises the primary reason for producing the computational model developed herein. It is envisioned that this model may be utilized in the future by railway engineers to assess the necessity for interventions or replacement of sections of the track structure for the purpose of avoiding costly and sometimes life-threatening track buckles. Toward this end, the present model has been deployed in order to demonstrate its application to realistic rail structures. It is envisioned that rail buckling mitigation strategies can be improved via sensitivity analyses and predictions of rail lift-off induced lateral buckling.

*Partially reproduced with permission from the authors, “Finite Element Formulation and Verification for Thermal Buckling of Rail Structures in the Horizontal Plane” by D Allen and G Fry [2017], CRR Report No. 2017-01

REFERENCES

D Allen and W Haisler (1985) Introduction to aerospace structural analysis, Wiley

D Allen (2013) Introduction to the mechanics of deformable solids: bars and beams, Springer

D Allen, G Fry and D Davis (2016) Development of a Model for Describing Nonlinear Lateral Resistance of Track Ballast, Technology Digest, TD-16-029

D Allen, G Fry (2017) Finite Element Formulation and Verification for Thermal Buckling of Rail Structures in the Horizontal Plane, CRR Report No. 2017-01

R.G Dong, S Sankar and R.V Dukkipati (1994) A Finite Element Model of Railway Track and its Application to the Wheel Flat Problem. Proceedings of the Institution of Mechanical Engineers, Part F: Journal of Rail and Rapid Transit, 208(1), 61–72.

L Euler (1744) Method inveniendi lineas curvas, Opera Omni, St. Petersburg, Russia

G Galileo (1637) Dialogues concerning two new sciences, Dover

G Grissom and A Kerr (2006) Analysis of lateral track buckling using new frame-type equations, Int J Mech Sci, 48:21-32

S Kaewunruen, T Lewandrowski and K Chamniprasart (2018) Dynamic Responses of Interspersed Railway Tracks to Moving Train Loads. International Journal of Structural Stability and Dynamics, 18, 1850011.

A Kerr (1974) The stress and stability analyses of railroad tracks, J Appl Mech, 41:841-848

A Kerr (1978) Analysis of thermal track buckling in the lateral plane, Acta Mechanica, 30:17-50

A Kerr (2000) On the determination of the rail support modulus k, International Journal of Solids and Structures 37(32):4335-4351

A Kish, and G Samavedam (1982) Analysis of Thermal Buckling Tests on United States Railroads, DOT/FRA/ORD-82/45

A Kish, G Samavedam and D Jeong (1985) Influence of Vehicle Induced Loads on the Lateral Stability of CWR Track, DOT/FRA/ORD-85/03

A Kish and G Samavedam (1997) Longitudinal Force Measurement in Continuous Welded Rail from Beam Column Deflection Response, AREA Bulletin 712, Vol. 88

A Kish and G Samavedam (1990) Analyses of Phase III Dynamic Buckling Tests, DOT/FRA/ORD-89/08

A Kish and G. Samavedam (1991) Dynamic Buckling Test Analyses of a High Degree CWR Track, DOT/FRA/ORD-90/13

A Kish and G Samavedam (1991) Dynamic Buckling of Continuous Welded Rail Track: Theory, Tests, and Safety Concepts, Transportation Research Record, 1289, Proceedings of Conference on Lateral Track Stability

A Kish, S Kalay, A Hazell, J Schoengart, and G Samavedam, (1993) Rail Longitudinal Force Measurement Evaluation Studies Using the Track Loading Vehicle, Bulletin 742, American Railway Engineering Association

A Kish, D.W Clark and W Thompson (1995) Recent Investigations on the Lateral Stability of Wood and Concrete Tie Tracks, AREA Bulletin 752, pp 248-265

A Kish and G Samavedam (1999) Risk Analysis Based CWR Track Buckling Safety Evaluations, Proceedings of Conference on Innovations in the Design and Assessment of Rail Track, Delft University of Technology, The Netherlands

A Kish, G Samavedam, and D Wormley (2001) New Track Shift Limits for High-Speed Rail Applications, World Congress for Railway Research (WCRR 2001), Cologne, Germany.

A Kish, T Sussman, and M Trosino (2003) Effects of Maintenance Operations on Track Buckling Potential, International Heavy Haul Association Technical Conference, Dallas, Texas.

A Kish and G Samavedam (2005) Improvements in CWR Destressing for Better Management of Rail Neutral Temperature, Transportation Research Board 2005 Annual Conference

A Kish and G Samavedam (2013). Track buckling prevention: theory, safety concepts, and applications (No. DOT/FRA/ORD-13/16). John A. Volpe National Transportation Systems Center (US).

J.W Klaren and J.C Loach (1965) Lateral Stability of Rails, Especially of Long Welded Rails, Question D14, ORE, Utrecht

S Kristoff (2001) Track Lateral Strength Measurements at Union Pacific Railroad Sites, Foster-Miller Report prepared for Union Pacific Railroad

S.R Li and R.C Batra (2007) Thermal buckling and postbuckling of Euler-Bernoulli beams supported on nonlinear elastic foundations. AIAA journal, *45*(3), 712-720.

N Lim, N Park and Y Kang (2003) Stability of continuous welded track, Computers & Structures, 81:2219-2236

D Little, D Allen and A Bhasin (2016) Modeling and Design of Flexible Pavements and Materials, Springer

A Miri et al. (2021) Analysis of Buckling Failure in Continuously Welded Railway Tracks, Engineering Failure Analysis, vol. 119, p. 104989, DOI: 10.1016/j.engfailanal.2020.104989.

Nippon Steel Corporation (2020) Rails, downloaded at: https://www.nipponsteel.com/product/catalog_download/pdf/K003en.pdf

J Oden and E Ripperger (1981) Mechanics of elastic structures, Second Edition, McGraw-Hill

G.P Pucillo (2016) Thermal buckling and post-buckling behavior of continuous welded rail track, Vehicle System Dynamics, 54:12, 1785-1807, DOI: 10.1080/00423114.2016.1237665

Railroad Accident Statistics (2020) Federal Railroad Administration, downloaded at:http://safetydata.fra.dot.gov/officeofsafety/publicsite/Query/TrainAccidentsFYCYWithRates.aspx

D Read, R Thompson, D Clark and E Gehringer (2011) Results of Union Pacific concrete tie track panel shift tests, Technology Digest, TD-11-004

J Reddy (1984) An Introduction to the Finite element Method, McGraw-Hill

J Reddy (2005) An Introduction to the Finite element Method, Third Edition, McGraw-Hill

G Samavedam (1979) Buckling and Post Buckling Analyses of CWR in the Lateral Plane, British Railways Board, R&D Division, Technical Note, TN TS 34

G Samavedam, A Kish and D Jeong (1986) Experimental Investigation of Dynamic Buckling of CWR Tracks, DOT/FRA/ORD-86/07

G Samavedam, A Kish and D Jeong (1987) The Neutral Temperature Variation of Continuous Welded Rails, AREA Bulletin 712

G Samavedam, A Purple, A Kish and J Schoengart (1993) Parametric Analysis and Safety Concepts of CWR Track Buckling, Final Report, DOT/FRA/ORD-93/26

G Samavedam (1995) Theory of CWR Track Stability, ERRI Report, D202/RP3, Utrecht

G Samavedam, A Kanaan, J Pietrak, A Kish and A Sluz (1995) Wood Tie Track Resistance Characterization and Correlations Study, Final Report, DOT/FRA/ORD-94/07

G Samavedam (1997) Investigation on CWR Longitudinal Restraint Behavior in Winter Rail Break and Summer Destressing Operations, DOT/FRA/ORD-97/01

G Samavedam et. al. (1997) Analysis of Track Shift Under High-Speed Vehicle-Track Interaction, Technical Report DOT/FRA/ORD-97/02

G Samavedam and A Kish (2002) Track Lateral Shift Model Development and Test Validation, DOT/VNTSC/FRA Report

E Selig, D Li (1994) Track Modulus: Its Meaning and Factors Influencing It, Transportation Research Record, No. 1470, Railroad Research Issues, http://onlinepubs.trb.org/Onlinepubs/trr/1994/1470/1470-006.pdf

S Timoshenko (1915) Strength of rails, Transactions of the Institute of Ways and Communications, St. Petersburg, Russia

S Timoshenko (1927) Method of analysis of statical and dynamical stresses in rail, Proc. Second International Congress for thermal track buckling, Int J Mech Sci, 23:577-587 Applied Mechanics, Zurich

V Tvergaard and A Needleman (1981) On localized thermal track buckling, Int J Mech Sci, 23:577-587

G Yang and M.A Bradford (2016) Thermal-induced buckling and postbuckling analysis of continuous railway tracks. International Journal of Solids and Structures, *97*, 637-649.